Cancer initiation is associated with sex-biased tissue environments and imbalances between estrogen receptor alpha and thyroid hormone receptors

Feng Zhang[1], Minghua Deng[1,2,3]*

Affiliations:

[1]Center for Quantitative Biology, Academy for Advanced Interdisciplinary Studies, Peking University, Beijing, China.
[2]School of Mathematical Sciences, Peking University, Beijing, China.
[3]Center for Statistical Science, Peking University, Beijing, China.
*Corresponding author.
Corresponding author email: dengmh@math.pku.edu.cn.
Corresponding author ORCID: https://orcid.org/0000-0002-9143-1898

Plain English summary

Sex bias has been long observed in cancer susceptibility and prognosis. Hormone difference between the two sexes was believed to play a role. However, the mechanism is still largely unknown. Our study has shown that the activity of one hormone secreted from pituitary, namely gonadotropin-releasing hormone, are correlated to sex-biased tissue environment, which was speculated to influence patterns of cancer initiation. Furthermore, hormonal imbalance, particularly imbalance in estrogen and thyroid hormone, which is associated with specific cancer subtypes, was speculated to influence the direction of cancer initiation.

Highlights

- There are two distinct patterns of cancer age-specific incidence curve between the two sexes: parallel and nonparallel.
- The nonparallel pattern is associated with sex-biased tissue environment which is associated with sex-biased activity of gonadotropin-releasing hormone.
- Three sex-biased mutated genes: *PTEN*, *PGM5* and *LARP4B*, have tissue-specific hotspot mutations which are associated with microsatellite instability (MSI), and the proportion of MSI exhibit sex bias in stomach cancer.
- Three hypoxia induce factors (HIFs) phases: hypoxia, hyperoxia, and "chaotic-oxia", exist in most cancers and are linked to specific cancer subtypes, including cancers with MSI, the CpG island methylator phenotype, and hypermethylation.
- The phases of HIFs are associated with imbalances between estrogen receptor alpha and thyroid hormone receptors.

Abstract

Background
There is extensive evidence of sex differences in the susceptibility and prognosis of non-reproductive cancers. In addition to external factors, biological sex bias (e.g., sex chromosomes, hormones, and immune function) is suspected to function as a selective pressure that influences the evolutionary process of cancer initiation. However, there remains a lack of clarity concerning the extent of the effect of sex bias on cancer initiation, as well as the underlying mechanism.

Methods
Using epidemiology data, we described patterns of cancer age-specific incidence curve and compared curve patterns between women and men across cancers. Using molecular data, such as mRNA expression and DNA mutation profiles, we describe and compare molecular signatures of cancers between women and men, and between different cancer subgroups.

Results
In this study, we show that tissue sex bias, correlated to gonadotropin-releasing hormone, varies among tissues and is associated with two distinct age-specific patterns of cancer incidence: parallel and nonparallel. Additionally, we reveal that imbalances in estrogen receptor alpha and thyroid hormone receptors are associated with levels of hypoxia-inducible factors, which have three phases (hypoxia, hyperoxia, and "chaotic-oxia") that exist in most cancers and are linked to specific cancer subtypes, including cancers with microsatellites, the CpG island methylator phenotype, or hypermethylation.

Conclusion
Our results suggest that sex-biased tissue environments and hormonal imbalances may influence the pattern and direction of cancer initiation, emphasizing the importance of maintaining hormonal homeostasis for cancer prevention and providing insights toward improving therapies for cancer types with hormonal imbalances.

Background

The age-specific incidence curve of a particular cancer can represent the evolutionary dynamics of cancer initiation. For carcinomas (i.e., most solid cancers), age-specific incidence curves are approximately linear on a log-log scale (1). Armitage and Doll proposed a multistage model explaining the power law relationship, based on the assumption that carcinogenesis is a multistage process involving the accumulation of driver mutations (2). This model has been modified by other studies to incorporate new information (3-8). Cancer initiation is influenced by selective pressure from the microenvironment, through a process in which driver mutations (genetic or epigenetic) are selected and accumulated. Generally, different cancer types have distinct mutational spectra (9, 10), indicating that variations in tissue environment and cell type can influence the evolutionary dynamics of cancer initiation.

For nearly all non-reproductive cancers, women and men have different susceptibilities and prognoses. However, behavior or mutagen exposure can only partly explain this phenomenon (11). Biological sex bias, involving sex chromosomes and hormones, also plays a role in many instances (12-15). Recent studies have shown that female and male patients preferentially exhibit mutations of certain genes and gain specific transcriptional or epigenetic signatures (16-18); because they display stronger immunity, female patients preferentially accumulate more mutant peptides that are not recognized by T cell receptors (19). These studies provide evidence to support the hypothesis that sex bias is a selective pressure with the potential to influence cancer initiation. However, the mechanism by which sex bias influences cancer initiation remains largely unknown.

Materials and methods

Epidemiology data processing

To ensure the reliability of our analysis, we selected regions with the top 10 GDP in 2005, corresponding to the CI5X database, which records incidence from 2003 to 2007. The GDP information was obtained from the World Bank database (https://databank.worldbank.org/). In the data of USA, we selected two cohorts - white and black - to cover the black race, resulting in a total of 11 cohorts of regions or races: USA black, USA white, Japan, Germany, England, China, France, Italy, Canada, Spain, and Korea. We then chose major non-reproductive cancers according to Cancer Statistics US (20): lung (LUSC and LUAD), melanoma, colon, bladder, kidney, pancreas, thyroid, rectum, liver, stomach, brain, esophagus, oral cavity and pharynx, gallbladder, and larynx. This resulted in a total of 11 by 16 cohorts included in our analysis.

To reduce noise in the incidence of adrenal gland cancer, we merged the regional cohorts into continent cohorts. Specifically, we merged the USA black, USA white, and Canada cohorts into a North America cohort, merged Japan, China, and Korea cohorts into an Asia cohort, and merged Germany, England, France, Italy, and Spain cohorts into a Europe cohort.

We cut the age-specific incidence data from 30 to 70 years of age. Because previous studies have shown that incidence rates before the age of 30 are higher than expected due to factors such as family inheritance, exposure to carcinogens, or explosive cell division during development (1, 21), and incidence rates after the age of 70 are lower than expected due to the selection of relatively unsusceptible individuals (22). We then used the least squares method to fit straight lines separately for women and men at a log-log scale.

Nonparallel pattern test

We consider a linear equation (equation 1) as below:

$$incidence = \alpha \cdot age + \beta \cdot sex + \lambda \cdot age \cdot sex + \varepsilon.$$

Denoting 0 as female and 1 as male, so the linear equation for male is:

$$incidence_{\text{male}} = \alpha \cdot age + \beta + \lambda \cdot age + \varepsilon.$$

The linear equation for female is:

$$incidence_{\text{female}} = \alpha \cdot age + \varepsilon.$$

When λ is 0, two lines of sexes are parallel, when λ is not 0, two lines of sexes are nonparallel. So, we perform a linear regression as equation 1, and test if λ is significant not equal to 0 (significant nonparallel, Student's t-test). Then P values are adjusted by Bonferroni methods, adjusted P values which lower that 0.05 are reported as significant.

Sex-biased expressed pathways analysis

Carcinomas typically originate from solid tissues. Therefore, in the GTEX data, we selected tissues from which major solid cancers originate and excluded blood and solid tissues that are less likely to develop cancer, such as heart and fat. After this selection process, we chose 12 tissues: bladder, kidney, liver, skin, colon, stomach, pancreas, lung, thyroid, brain, esophagus, and adrenal gland. The number of samples for each tissue is shown in Table S1.

We obtained human pathway information using the R package KEGGREST (23, 24), resulting in a total of 352 pathways included in our analysis.

To ensure that each tissue had equal testing power for comparison between tissues, we randomly selected 100 samples from each tissue and conducted sex-biased expressed pathways analysis. For each pathway, we used the mean logarithmic expression [log (counts+1)] of all genes in the pathway as the expression strength of the pathway. We divided the samples in each tissue into two groups based on sex and compared pathway expression strength between groups using Limma, while correcting for the factor of the position of the tissue (body site detail). As shown in Table S1, there was a large difference in sample size between tissues, and our approach allowed us to account for these differences and ensure that our analysis was statistically robust.

Our analysis was affected by poor testing power due to both the expression strength of the pathway, the mean expression of all genes, can weaken the real signal of a set of specific genes in that pathway, and the small sample size resulting from our sampling approach. However, as we only made qualitative comparisons, we relaxed the significance standard and considered unadjusted P values < 0.05 to be significant. We then recorded the number of significantly different pathways in each tissue. This analysis process was repeated 1000 times, and the numbers of sex-biased expressed pathways in each tissue were displayed in Figure 2.1C. As the samples from bladder and kidney were less than 100, and they had no significant sex-biased expressed pathways, their final statistical results were marked as NA.

Mutation data processing for sex-biased mutated gene test

We used MC3 profile of TCGA mutation data. We excluded pediatric and blood cancers, as well as sex-specific cancers, leaving only non-reproductive adult solid tumors.

To filter out passenger mutations and reduce data noise, we performed filtering on the mutation data. Firstly, we retained mutations of the following types: nonsense, insertion, deletion, translation start site, and non-stop mutations, as these mutations would theoretically change the protein sequence. We also retained mutations predicted as "deleterious" by SIFT (25) and as "probably damaging" by PolyPhen (26). In addition, we retained mutations at a single site where mutations occurred five or more times in the entire MC3 dataset.

To reduce potential statistical bias from extremely high mutation samples, we removed the top 5% of samples with the highest tumor mutation burden (TMB) for each cancer type. Additionally, we removed genes with a sample mutation rate below 5%, as these genes have

limited biological significance and their removal can improve the power of a statistical test. For the analysis of melanoma, which is only susceptible in white populations and typically only has nonparallel patterns in white populations, we only considered the white population.

Likelihood ratio test

Based on our preliminary analysis of sex-biased mutated genes using the Fisher exact test and the conclusions from previous work (27), we identified tumor mutation burden (TMB) as an important confounding factor for testing sex-biased mutated genes, as there are sex-biased TMB in many cancers. Failure to exclude this confounding factor can result in many false positives, particularly for super long genes. To address this issue, we used a likelihood ratio test (LRT) similar to previous work (17) to eliminate the confounding factor of TMB. The LRT also corrected for the difference in copy numbers of the X chromosome between men and women.

The background mutation rate varies between samples. Firstly, we assumed that the mutation rate of a gene between male and female samples is unbiased. Therefore, the mutation rate ratio of a gene between male and female samples should be approximately equal to the background mutation rate ratio between male and female samples. We formulated the null hypothesis that the mutation rate of a gene is not biased between male and female samples. In other words, if the null hypothesis is true, for each gene:

$$p_{female} = \lambda \cdot p_{male}.$$

Where P_{female} is the mutation rate of a gene in female samples, P_{male} is the mutation rate of a gene in male samples, and λ is the background mutation rate ratio between male and female samples. We defined the mutation rate of a gene as the ratio of samples with mutations in that gene divided by the total number of female or male samples in a given cancer type. We denoted the mutation rate of a gene in female samples as P_{female} and the mutation rate of the same gene in male samples as P_{male}. The background mutation rate ratio for a gene was defined as the ratio of the total number of mutations on the chromosome where the gene is located in female samples to the total number of mutations on the same chromosome in male samples.

Under the assumption that the null hypothesis is true, the likelihood function is:

$$L_0 = \max\left((\lambda \times p_{male})^f \times (1 - \lambda \times p_{male})^{F-f} \times {p_{male}}^m \times (1 - p_{male})^{M-m} \right).$$

If the null hypothesis is not true, it is assumed that P_{male} and P_{female} are not proportional to each other, and the likelihood function is:

$$L_1 = \max\left({p_{female}}^f \times (1 - p_{female})^{F-f} \times {p_{male}}^m \times (1 - p_{male})^{M-m} \right).$$

The log-likelihood ratio (LLR) is then calculated as:

$$LLR = \ln\left(\frac{L_1}{L_0} \right).$$

According to Wilks' theorem, 2×LLR follows a chi-square distribution with one degree of freedom. Thus, we can calculate the P value, and the P value for each gene is adjusted using the Benjamini-Hochberg method within each cancer types.

Logistic regression analysis

To account for potential confounding factors such as age, cancer grade, smoking history, and alcohol history, we conducted logistic regression analysis with these covariates to investigate the significance of sex in gene mutations.

We used the likelihood ratio test to identify genes with adjusted P values below 0.05, which helped eliminate the confounding factor of tumor mutation burden (TMB) and chromosome copy number. We also used logistic regression analysis with a significance threshold of $P < 0.05$ to identify genes that were significant after accounting for confounding factors. Genes that were identified as significant by both the likelihood ratio test and logistic regression analysis were reported as significant genes.

Test for sex biased mutated genes on Y chromosome

As women do not possess the Y chromosome, the LRT method cannot be employed for genes located on the Y chromosome. Therefore, we utilized the Fisher exact test to evaluate the significance of mutations in genes located on the Y chromosome. We adjusted the resulting P values using the Benjamini-Hochberg method to account for multiple testing. Genes with an adjusted P value below 0.05 were considered significant.

Subtype labeling in TCGA data and sample grouping

We obtained sample subtypes in TCGA from the molecular subtype profiles available on UCSC Xena (28). We used the following sample groupings for our analysis.

For STAD and COAD, we grouped samples labeled "HM-indel" or "HM-SNV" in the MSI+ group, while samples labeled "CIN", "GS", or "EBV" were grouped in the MSI- group. These sample groupings match well with the samples labeled "msi-h" in previous study (29). For UCEC, we grouped samples labeled "UCEC.POLE" or "UCEC.MSI" in the MSI+ group, while samples labeled "UCEC.CN_LOW" or "UCEC.CN_HIGH" were grouped in the MSI- group.

For LGG and ACC, samples labeled "CIMP-high" were grouped in the HyperMeth group, while samples labeled "CIMP-low" were grouped in the HypoMeth group. For THCA, samples labeled "CpG island methylated" were grouped in the HyperMeth group, while samples labeled "follicular" were grouped in the HypoMeth group. For SKCM and HNSC, samples labeled "CpG island-methylated" or "hyper-methylated" were grouped in the HyperMeth group, while samples labeled "normal-like" or "hypo-methylated" were grouped in the HypoMeth group. For PCPG, samples labeled "hyper-methylated" were grouped in the HyperMeth group, while samples labeled "low-methylated" were grouped in the HypoMeth group. For LUAD, samples labeled

"high" were grouped in the HyperMeth group, while samples labeled "low" were grouped in the HypoMeth group. For PRAD, samples labeled "1" were grouped in the HyperMeth group, while samples labeled "4" were grouped in the HypoMeth group.

For BRCA, samples labeled "LumA" or "LumB" were grouped in the ER+ group, while samples labeled "Her2" or "Basal" were grouped in the ER- group.

Differentially expressed genes (DEGs) analysis

We conducted DEGs analyses using Limma between two groups in each cancer type with enough labeled samples (more than 50). Specifically, we compared HOTSPOT+ versus HOTSPOT- in STAD, COAD, and UCEC; MSI+ versus MSI- in STAD, COAD, and UCEC; HyperMeth versus HypoMeth in HNSC, LUAD, PRAD, ACC, PCPG, LGG, THCA, and SKCM; and ER+ versus ER- in BRCA. We corrected for covariates such as sex, age, tumor stage, race, alcohol, and smoking history during the DEG analyses.

We created two pseudogenes, THR and HIF, to represent thyroid hormone receptor level and hypoxia level, respectively, in each sample. Pseudogene THR was created by using the summed logarithmic counts of *THRA* and *THRB*, while pseudogene HIF was created by using the logarithmic counts of *HIF1A* minus the logarithmic counts of *HIF3A*. Both THR and HIF were analyzed together with all the other genes during the DEG analyses.

We reported the adjusted P value and log fold change (logFC) provided by Limma for each gene. Specifically, genes with a Limma adjusted P value lower than 0.05 and an absolute value of logFC higher than 1 were considered significant.

Sets of genes focused in expression signature

Basing on the role of GnRH on tissue sex bias and the crosstalk between HPG, HPA and HPT axes and relationship between *ESR1* and hypoxia, we focused on the following sets of genes: GnRH (*GNRH1*) and its receptors (*GNRHR*, *GNRHR2*), glycoprotein hormones alpha polypeptide (*CGA*), luteinizing hormone (*LHB*) and its receptors (*LHCGR*), follicle stimulating hormone (*FSHB*) and its receptor (*FSHR*), thyrotropin releasing hormone (*TRH*) and its receptor (*TRHR*), thyroid stimulating hormone (*TSHA*, *TSHB*) and its receptor (*TSHR*), corticotrophin-releasing hormone (*CRH*) and its receptor (*CRHR1* and *CRHR2*), adrenocorticotropic hormone (*POMC*) and its receptor (*MC2R*), glucocorticoid receptor (*NR3C1*), thyroxine-binding globulin (*SERPINA7*), transthyretin (*TTR*), estrogen receptors (*ESR1*, *ESR2*), thyroid hormone receptors (*THRA*, *THRB*), testis receptor (*NR2C1*, *NR2C2*), androgen receptor (*AR*), progesterone receptor (*PGR*), hypoxia-inducible factors (*HIF1A*, *EPAS1*, *HIF3A*, *EGLN1*, *EGLN2*, *EGLN3*, *ARNT*).

Results

Parallel and nonparallel patterns of age-specific cancer incidence in women and men

Based on the hypothesis that sex bias influences cancer initiation which can be represented by the age-specific incidence curve of a particular cancer, we used the CI5-X database (provided by the International Agency for Research on Cancer) to compare the incidence curves of major solid cancer types between women and men in selected regions or ethnicities (see methods). Fitted age-specific incidence curves for men and women showed two general patterns on a log-log scale: parallel and nonparallel (Fig. 1A). Parallel patterns were observed when colon cancer incidences were compared between inherited and sporadic types (7), and when lung cancer incidences were compared between smokers and non-smokers (30). These parallel patterns suggest that individuals with a susceptible genetic background or greater exposure to mutagens have a higher baseline risk of cancer. To our knowledge, nonparallel patterns have not been reported.

To determine the prevalence of nonparallel patterns in major solid cancers according to region or ethnicity, we conducted a linear regression analysis and explored age-by-sex interactions to determine the statistical significance of the nonparallel pattern in each cohort (see methods). Our analysis revealed that nonparallel patterns were more common in stomach cancer, melanoma, and thyroid cancer (Fig. 1B).

Sex bias in tissue environments

A potential explanation for the prevalence of nonparallel patterns is that tissue environments in the stomach, skin, and thyroid exhibit greater sex differences compared with tissue environments in the other regions; these differences may influence cancer initiation. To test this hypothesis, we used GTEx data to evaluate sex bias in tissue environments via sex-biased expressed pathway analysis. In our analysis, the level of expression in a pathway was represented by the mean level of expression for all genes in that pathway; we randomly selected 100 samples from each tissue to maintain consistent statistical power across tissues. We explored sex-biased expressed pathway using Limma (31); we repeated this process 1000 times and recorded the numbers of sex-biased expressed pathways in each tissue during each repetition (see methods). There were fewer than 100 kidney and bladder samples (Table S1) and no significant sex-biased expressed pathways were identified in those tissues; thus, their results were regarded as not available (NA). The results showed that the adrenal glands, stomach, thyroid, and skin contained the largest numbers of sex-biased expressed pathways (Fig. 2A).

To determine which pathways have greater involvement in tissue sex bias, we re-examined sex-biased expressed pathways using all samples in each type of tissue except the bladder, for which only nine samples were available. Among the pathways, only the gonadotropin-releasing hormone (GnRH) secretion pathway (hsa04929) exhibited significant sex bias (Limma $P < 0.05$) in the top three tissues with sex bias (adrenal glands, thyroid, and stomach), but not in other tissues (P for skin = 0.0683, Table S2). Additionally, the female-to-male log fold change (LogFC) of the GnRH secretion pathway were highest in the adrenal glands, stomach, and thyroid; the LogFC in skin was fifth highest (Fig. 2B). The LogFC of the GnRH secretion pathway was positively correlated (Pearson correlation coefficient $R = 0.74$) with the number of sex-biased expressed pathways in each tissue. The LogFC of another GnRH-related pathway, the GnRH signaling pathway (hsa04912), was also positively correlated (Pearson correlation coefficient $R = 0.91$) with the number of sex-biased expressed pathways in each tissue. The

adrenal glands, stomach, and thyroid had the highest LogFCs, whereas the skin had a negative LogFC (Fig. 2C, Table S3).

Adrenal gland cancer is a rare type of cancer, and linear representation of its age-specific incidence is hindered by noise. Therefore, it was not included in the nonparallel analysis shown in Figure 1B. However, because adrenal gland tissue had the highest number of sex-biased expressed pathways and largest LogFC of the two GnRH-related pathways, we repeated the nonparallel pattern analysis with a focus on adrenal gland cancer. To reduce noise in the incidence of adrenal gland cancer, we merged the regional cohorts into continental cohorts (see methods). We found that adrenal cancer incidence also displayed a nonparallel pattern; the results were statistically significant in North America and Asia cohorts (Fig. 2D).

The most prevalent nonparallel patterns in stomach cancer, melanoma, thyroid cancer, and adrenal cancer were observed across regions or ethnicities (Figs. 1B and 2D). Consistent with these findings, adrenal glands, stomach, thyroid, and skin exhibited the highest numbers of sex-biased expressed pathways (Fig. 2A), which were associated with GnRH-related pathways. Thus, sex-biased tissue environments may influence the evolutionary dynamics of cancer initiation and induce nonparallel patterns.

Genes with sex-biased mutation frequency

Because cancer initiation can be influenced by sex, there may exist genes that exhibit a greater likelihood of mutation in a single sex (hereafter, “sex-biased mutated genes”). Previous studies attempted to explore this hypothesis, but they had less statistical power because of reliance on incomplete The Cancer Genome Atlas (TCGA) data (16, 17) or whole genome sequencing data alone (18). Therefore, we used complete TCGA data to conduct a comparative analysis of gene mutation frequency between women and men among 6181 individuals across 24 non-reproductive cancers; we utilized both the likelihood ratio test (LRT) and logistic regression analysis to adjust for confounding factors (see methods). Our results revealed eight sex-biased mutated genes (Table 1): *DNAH7*, *LARP4B*, *PGM5*, and *PTEN* in stomach adenocarcinoma (STAD); *SELP* and *SPAG17* in skin cutaneous melanoma (SKCM); *RBM10* in lung adenocarcinoma (LUAD); and *CASP8* in head and neck squamous cell carcinoma (HNSC).

Hotspot dominance in three sex-biased mutated genes in STAD

In STAD, three sex-biased mutated genes (*PTEN*, *LARP4B*, and *PGM5*) displayed hotspot mutation dominance, as shown in Figure 3 [depicted using ProteinPaint (32)]. These hotspots, Lys267ArgfsTer9 (c.800delA) in *PTEN*, Thr163HisfsTer47 (c.487delA) in *LARP4B*, and Ile98Val (c.292A>G) in *PGM5*, also showed a significant sex bias ($P < 0.05$, Fisher’s exact test, Fig. 3). TCGA data showed that these three hotspots were exclusively present in STAD, colon adenocarcinoma (COAD), and uterine corpus endometrial carcinoma (UCEC), with the exception of a *PGM5* hotpot in prostate adenocarcinoma (PRAD). The mutational spectra of other sex-biased mutated genes are shown in Figure S1.

Sex-biased hotspots and sex-biased proportions of cancers with microsatellite instability (MSI)

To determine the underlying cause of sex bias in the presence of the three hotspots, we conducted co-occurrence and mutual exclusivity analyses of the three hotspots in STAD, COAD, and UCEC; the results suggested that the three sex-biased hotspots tend to co-occur (Table S4). To gain further insight, we divided the samples into two groups (HOTSPOT+ and HOTSPOT-) according to the presence or absence of at least one of the three hotspots across STAD, COAD,

and UCEC. Subsequently, we used Limma to conduct an analysis of differentially expressed genes (DEGs) between the two groups.

In all three cancers, four genes were differentially expressed between the two groups: *C7orf31*, *MLH1*, *EPM2AIP1*, and *LINC00667* (Fig. S2A, Data S4). *MLH1*, a well-known tumor suppressor gene, showed reduced expression in the HOTSPOT+ group across all three cancers (Fig. S2B). *MLH1* deficiency can induce MSI, which is commonly observed in colorectal, gastric, and endometrial cancer. The signatures of the three hotspots were consistent with previously reported mutational signatures of MSI cancer types: the *PTEN* and *LARP4B* hotspots are typical of the MSI mutational signature ID1, whereas the *PGM5* hotspot is typical of the MSI mutational signatures SBS21 and SBS26 (33). Furthermore, all HOTSPOT+ samples were labeled as the MSI subtype in TCGA data (see methods). This evidence suggests that the three hotspots result from hypermutation across MSI subtypes.

We speculated that hotspot-specific sex bias is caused by sex bias in MSI subtype. Thus, we examined MSI subtype proportions in STAD and COAD; in both cancers, we found that the MSI subtype proportion was higher in women than in men. The difference was statistically significant in STAD (Table S5). A previous study (34) revealed that, in both gastric and colorectal cancers, the MSI subtype proportion was significantly higher in women than in men (Table S6).

Estrogen receptor alpha (*ESR1*), thyroid hormone receptors (THRs), and hypoxia-inducible factors (HIFs) in cancers with MSI

The above findings led us to investigate the underlying cause of sex bias in MSI subtype. For this purpose, we divided STAD, COAD, and UCEC samples into two groups: MSI-positive (MSI+) and MSI-negative (MSI-). We then analyzed DEGs in each cancer type (see methods).

Hypoxia is known to suppress mismatch repair through mechanisms such as the reduction of *MLH1* expression (35-38). In STAD, COAD, and UCEC, we observed that MSI+ samples consistently had a significantly elevated level of *HIF1A* (a key activator of hypoxia signaling) or a reduced level of *HIF3A* [a repressor of hypoxia signaling (39)], compared with MSI- samples. These findings indicated that MSI+ samples had a higher level of hypoxia. Subsequently, we used the ratio of *HIF1A* to *HIF3A* (i.e., HIF level), to represent the level of hypoxia in each sample. We found that the HIF level was significantly higher in MSI+ samples than in MSI- samples; it was positively correlated with the *MLH1* methylation level in all three cancers (Fig. 4A).

ESR1 has been reported that it can directly regulates *HIF1A*, indicating crosstalk between the hypoxia and estrogen signaling pathways (40). However, in STAD, COAD, and UCEC, we found that the level of *ESR1* did not significantly differ between MSI+ and MSI- samples. Furthermore, the expression of *ESR1* was positively correlated with the HIF level in UCEC, but not in STAD or COAD (Figs. 4B and 5A). Finally, pan-cancer analysis of TCGA data showed that *ESR1* only had a slight positive correlation with the HIF level; conversely, pan-tissue analysis of GTEx data revealed a negative correlation with the HIF level (Fig. S3).

Our above results indicated that GnRH was involved in the establishment of a sex-biased tissue environment. GnRH is a key regulator of the hypothalamic-pituitary-gonadal (HPG) axis, which is upstream of estrogen signaling and has substantial crosstalk with the hypothalamic-pituitary-adrenal (HPA) and hypothalamic-pituitary-thyroid (HPT) axes (41). Considering these connections, besides *ESR1*, we suspected that other hormones or hormone

receptors were involved in the sex bias in MSI subtype. Therefore, we investigated the expression patterns of a set of genes involved in the HPG, HPA, and HPT axes (see methods).

The results showed that only one gene, thyroid hormone receptor beta (*THRB*), was significantly differentially expressed between MSI+ and MSI- samples in all three cancer types. Moreover, thyroid hormone receptor alpha (*THRA*) was significantly differentially expressed in STAD and COAD, but not in UCEC (Fig. S4, Data S5). Because *THRA* and *THRB* are both important receptors for thyroid hormone (TH), we used the summed logarithmic levels of *THRA* and *THRB* to represent the THR level in each sample. We found that the THR level was significantly lower in MSI+ samples than in MSI- samples; it was negatively correlated with the HIF level in all three cancers (Fig. 4C). The negative correlation between HIF and THR was also confirmed by pan-cancer analysis of TCGA data and pan-tissue analysis of GTEx data (Fig. 4D).

ESR1, THR, and HIF in cancers with hypermethylation or in estrogen receptor-positive (ER+) breast cancers (BRCAs)

Epigenetic silencing of the *MLH1* gene is a major cause of MSI; it can occur in cancers with the CpG island methylator phenotype (CIMP) or hypermethylation. There is a significant overlap between colorectal cancers with MSI and colorectal cancers with CIMP (42). Accordingly, to explore whether cancers with CIMP or hypermethylation exhibit expression signatures similar to MSI+ cancers (e.g., *ESR1*, THR, and HIF), we conducted a similar analysis of cancers with sufficient CIMP or hypermethylation labels in the TCGA dataset. These cancers were designated "HyperMeth cancers," whereas other cancers were designated "HypoMeth cancers" (see methods).

Based on their expression signatures, HyperMeth cancers were divided into two subgroups: hypoxia and hyperoxia. In the hypoxia subgroup, similar to MSI+ cancers, all HyperMeth cancers demonstrated a significantly elevated HIF level (except HyperMeth SKCM, in which the increase was not statistically significant); they typically had a reduced THR level or an elevated *ESR1* level (Figs. 5A and S6). In the hyperoxia subgroup, all HyperMeth cancers demonstrated a significantly reduced HIF level (except HyperMeth THCA, in which the decrease was not statistically significant); they also had a significantly elevated THR level or a significantly reduced *ESR1* level (Fig. 5A).

Adrenocortical carcinoma (ACC) and pheochromocytoma and paraganglioma (PCPG) both originate from adrenal glands. However, HyperMeth ACC and HyperMeth PCPG displayed opposing THR and HIF expression signatures. Specifically, HyperMeth ACC exhibited hypoxia, whereas HyperMeth PCPG exhibited hyperoxia. This difference suggests that the two cancers originated under divergent selective pressures or evolved in opposite directions.

BRCA is classified into four well-characterized molecular subtypes: luminal A, luminal B, HER2-positive, and triple-negative. Estrogen plays a crucial role in the development of ER+ BRCAs (i.e., luminal A and luminal B). To investigate whether ER+ BRCAs exhibit hypoxia and have expression signatures similar to MSI+ or hypoxic HyperMeth cancers, we compared expression signatures between ER+ BRCAs and ER- (i.e., HER2-positive and triple-negative) BRCAs. In contrast to the findings in MSI+ and HyperMeth cancers, we observed an antagonistic expression pattern in ER+ BRCAs: *ESR1* and THR levels were both significantly elevated, whereas the HIF level did not significantly differ (Fig. 5A). However, the *HIF1A* level tended to be significantly reduced, and the *HIF3A* level was significantly reduced (Fig. S5).

Estrogen receptor beta (*ESR2*) is also involved in hypoxia signaling. However, its role is not well established, and it exhibits opposing roles in some cancers (43). Our results showed that *ESR2* was significantly elevated in MSI+ COAD and significantly reduced in HyperMeth SKCM, indicating that *ESR2* may play a role in the initiation of these cancers.

Additionally, similar to the three hotspot mutations exclusively found in MSI+ cancers, some other sex-biased mutated genes tend to be present in certain cancer subtypes. Specifically, *CASP8* was typically mutated in HyperMeth HNSC, *SELP* was typically mutated in HyperMeth SKCM, and *DNAH7* was typically mutated in MSI+ STAD. These results were statistically significant (Table S7), suggesting a link between these sex-biased mutated genes and the corresponding cancer subtypes.

Imbalances in estrogen and TH may contribute to carcinogenesis

The above results imply that a sex-biased tissue environment can influence cancer initiation. *ESR1* and THR are associated with the HIF level in cancers, as well as specific cancer subtypes, suggesting that they also play a role in cancer initiation. *ESR1* can directly regulate *HIF1A* and induce the hypoxia signaling pathway (40). TH has a more complex role in hypoxia. TH can induce *HIF1A* activity, which then reduces TH signaling; however, experimental and clinical studies have revealed that TH plays a critical role in protecting tissues from hypoxic injury (44). We also observed this complex phenomenon: analysis of GTEx data revealed that the THR level was negatively correlated with the *HIF1A* level but positively correlated with the *HIF3A* level (Fig. S7). However, analysis of TCGA data demonstrated that the negative correlation between THR and *HIF1A* disappeared, whereas the positive correlation between THR and *HIF3A* persisted (Fig. S8). These results indicated that THR generally functions as a hypoxia repressor in cancers, rather than a hypoxia activator, similar to its protection against hypoxic injury.

ERs and THRs are both nuclear receptors with similar DNA-binding sequences. They can competitively bind to each other's DNA-binding sites and inhibit subsequent transcription (45). The mutual antagonism of ERs and THRs is consistent with the observations in Figure 5A: an increase in *ESR1* or a decrease in THR is accompanied by hypoxia, whereas a decrease in *ESR1* or an increase in THR is accompanied by hyperoxia.

Based on the present findings, we propose a model of carcinogenesis that involves imbalances in estrogen and TH (Fig. 5B). As noted above, TH and estrogen play key roles in many aspects of biological processes and maintain homeostasis under healthy conditions. However, TH or estrogen dominance can induce changes in the tissue environment, such as hypoxia or hyperoxia; it can also alter the epigenome and transcriptome in tissue cells. In ER+ BRCAs, both TH and estrogen can become simultaneously elevated, resulting in a state of antagonism or "chaotic-oxia." In terms of selective pressure for cancer evolution, all of these altered tissue environments can induce specific cancer subtypes, as shown in Figure 5A and B.

Discussion

The present study showed that cancer initiation may be influenced by sex bias in two ways: sex-biased tissue environments and hormonal imbalances. However, these influences are not mutually exclusive and may interact with each other. Here, we found that GnRH was associated with a sex-biased tissue environment; GnRH is a key regulator of the HPG axis and receives negative feedback from gonadal steroids, such as estrogen (46). The HPG axis has extensive crosstalk with the HPT axis, such as crosstalk between the estrogen and TH signaling pathways (41, 45). Together, the HPG axis and HPT axis, including estrogen and thyroid hormones, regulate tissue environment homeostasis. Generally, the level of estrogen is higher in women than in men (47); this increases the likelihood of a hypoxic tissue environment in women and the potential for cancers with MSI. As expected, we found that women had a higher prevalence of MSI in STAD and COAD; we also found that women had a high prevalence of MSI in UCEC, where estrogen is suspected to promote cancer progression (Table S5 and S6). In contrast, the lower level of estrogen in men increases the likelihood of a hyperoxic tissue environment in men and the potential for cancers such as the hyperoxic CIMP subtype of thyroid carcinoma. Although the difference was not statistically significant (possibly because of the small sample size), we found that men had a higher prevalence of the hyperoxic CIMP subtype of thyroid carcinoma (Table S5). However, we found that the hypoxic HyperMeth subtype of HNSC was more prevalent in men, indicating that it may exhibit tissue-specific regulation. These results suggest that in the context of sex-biased tissue environments and hormonal imbalances, cancer precursors have a preferred evolutionary trajectory. Consistent with this hypothesis, we observed that six of the eight sex-biased mutated genes were significantly enriched in specific cancer subtypes (Table S7). However, in cancers such as PCPG and SKCM, the proportions of subtypes were similar in women and men.

In addition to influencing the direction of cancer evolution, sex-biased tissue environments and hormonal imbalances may also affect the evolutional pace of cancer initiation. GnRH secretion exhibits pulsatile behavior in both men and women, but the frequency and amplitude of pulses in women are dependent on the phase of the menstrual cycle which do not exist in men (46). The sex-biased dynamics of GnRH secretion may lead to sex-biased dynamics of cancer evolution. Hypermutation or hypermethylation, which occur in cancers with hormonal imbalances, could lead to more rapid cancer evolution and altered dynamics of cancer initiation, as described in a previous study (6). All of these factors may contribute to the nonparallel pattern of cancer incidence observed in this study. However, greater understanding of sex-biased biological mechanisms is needed to develop a detailed mathematical model to explain the sex bias underlying the two patterns of age-specific cancer incidence.

TH is suspected to play a role in cancer initiation. For example, compared with men, women are 10-fold more likely to develop hyperthyroidism and hypothyroidism (48); these disorders have been linked to changes in the incidence and prognosis of many cancers (49). The present findings support the increasing importance of TH in cancer research. Although our study focused on the balance between TH and estrogen, we acknowledge that other hormones may also contribute to cancer initiation. For example, progestogen is reportedly involved in luminal A BRCA, and androgens have been linked to prostate cancer.

In this study, samples were grouped by molecular clustering labels, which may not fully capture the status of the balance between estrogen and TH. The identification of molecular patterns associated with imbalances in estrogen and TH could enhance our findings and reveal additional mechanisms involving sex bias. Furthermore, the levels of ERs and THRs may not directly

reflect the levels of estrogen and TH. Nevertheless, this study showed that three phases (hypoxia, hyperoxia, and chaotic-oxia) are present in most cancers and are linked to hormonal imbalances.

Perspective and significance

Altogether, our results identify two distinct patterns of age-specific cancer incidence between the two sexes, and link these patterns to sex-biased tissue environment, suggesting sex-biased tissue environment can influence the pattern of cancer initiation. Furthermore, we find ESR1 and THRs imbalances are associated with HIFs phases and specific cancer subtype, suggesting ESR1 and THRs imbalances can influence the direction of cancer initiation. These findings emphasize the importance of maintaining hormonal homeostasis for cancer prevention and provide insights toward improving therapies for cancer types that involve in hormonal imbalances.

Declarations

Ethics approval and consent to participate:

Research was carried out on data obtained from public data. No ethical approval was necessary as part of accessing these data.

Consent for publication:

Not applicable for this work.

Data availability:

The results published here are based on data generated by the TCGA Research Network (https://www.cancer.gov/tcga), the Genotype-Tissue Expression (GTEx) Project (https://www.gtexportal.org), UCSC Xena (https://xenabrowser.net/datapages), and the IARC database (http://ci5.iarc.fr/CI5-X/Pages/download.aspx). The analysis code is archived on GitHub (https://github.com/WhitePredator/sex-bias-in-cancer-initiation).

Competing interests:

The authors declare no competing interests.

Funding:

This work was supported by the National Key Research and Development Program of China (no. 2021YFF1200902) and the National Natural Science Foundation of China (nos. 32270689 and 12126305).

Author contributions:

F.Z. performed data processing, data analysis, interpreted the data, and prepared the manuscript. M.D. acquired funding, supervised the study, and reviewed the manuscript.

Acknowledgements:

The authors thank Minping Qian, Hong Wu, Zexian Zeng, Ruibin Xi, Donglai Wang, Ge Gao, Qing Li, Chao Tang, Jinzhi Lei, Yihan Lin, and Zemin Zhang for insightful discussions.

References

1. Nordling CO. A New Theory on the Cancer-Inducing Mechanism. British Journal of Cancer. 1953;7(1):68-72.
2. Armitage P, Doll R. The Age Distribution of Cancer and a Multi-Stage Theory of Carcinogenesis. British Journal of Cancer. 1954;8(1):1-12.
3. Knudson AG. Mutation and Cancer - Statistical Study of Retinoblastoma. P Natl Acad Sci USA. 1971;68(4):820-&.
4. Nowell PC. The clonal evolution of tumor cell populations. Science. 1976;194(4260):23-8.
5. Fearon ER, Vogelstein B. A Genetic Model for Colorectal Tumorigenesis. Cell. 1990;61(5):759-67.
6. Michor F, Iwasa Y, Nowak MA. Dynamics of cancer progression. Nat Rev Cancer. 2004;4(3):197-205.
7. Frank SA. Age-specific incidence of inherited versus sporadic cancers: A test of the multistage theory of carcinogenesis. P Natl Acad Sci USA. 2005;102(4):1071-5.
8. Meza R, Jeon J, Moolgavkar SH, Luebeck EG. Age-specific incidence of cancer: Phases, transitions, and biological implications. P Natl Acad Sci USA. 2008;105(42):16284-9.
9. Vogelstein B, Papadopoulos N, Velculescu VE, Zhou SB, Diaz LA, Kinzler KW. Cancer Genome Landscapes. Science. 2013;339(6127):1546-58.
10. Martincorena I, Campbell PJ. Somatic mutation in cancer and normal cells. Science. 2015;349(6255):1483-9.
11. Jackson SS, Marks MA, Katki HA, Cook MB, Hyun N, Freedman ND, et al. Sex disparities in the incidence of 21 cancer types: Quantification of the contribution of risk factors. Cancer-Am Cancer Soc. 2022;128(19):3531-40.
12. Clocchiatti A, Cora E, Zhang Y, Dotto GP. Sexual dimorphism in cancer. Nat Rev Cancer. 2016;16(5):330-9.
13. Rubin JB, Lagas JS, Broestl L, Sponagel J, Rockwell N, Rhee G, et al. Sex differences in cancer mechanisms. Biol Sex Differ. 2020;11(1).
14. Lopes-Ramos CM, Quackenbush J, DeMeo DL. Genome-Wide Sex and Gender Differences in Cancer. Front Oncol. 2020;10.
15. Oliva M, Munoz-Aguirre M, Kim-Hellmuth S, Wucher V, Gewirtz ADH, Cotter DJ, et al. The impact of sex on gene expression across human tissues. Science. 2020;369(6509):1331-+.
16. Yuan Y, Liu LX, Chen H, Wang YM, Xu YX, Mao HZ, et al. Comprehensive Characterization of Molecular Differences in Cancer between Male and Female Patients. Cancer Cell. 2016;29(5):711-22.
17. Dunford A, Weinstock DM, Savova V, Schumacher SE, Cleary JP, Yoda A, et al. Tumor-suppressor genes that escape from X-inactivation contribute to cancer sex bias. Nature Genetics. 2017;49(1):10-6.
18. Li CH, Prokopec SD, Sun RX, Yousif F, Schmitz N, Subtypes PT, et al. Sex differences in oncogenic mutational processes. Nat Commun. 2020;11(1):4330.

19. Castro A, Pyke RM, Zhang XL, Thompson WK, Day CP, Alexandrov LB, et al. Strength of immune selection in tumors varies with sex and age. Nat Commun. 2020;11(1).

20. Siegel RL, Miller KD, Jemal A. Cancer statistics, 2019. Ca-a Cancer Journal for Clinicians. 2019;69(1):7-34.

21. Nunney L. Commentary: The multistage model of carcinogenesis, Peto's paradox and evolution. Int J Epidemiol. 2016;45(3):649-U67.

22. Moolgavkar SH. Commentary: Fifty years of the multistage model: remarks on a landmark paper. Int J Epidemiol. 2004;33(6):1182-3.

23. Tenenbaum D, Maintainer B. KEGGREST: Client-side REST access to the Kyoto Encyclopedia of Genes and Genomes (KEGG). R package version 1.38.0. 2022.

24. Kanehisa M, Goto S. KEGG: Kyoto Encyclopedia of Genes and Genomes. Nucleic Acids Res. 2000;28(1):27-30.

25. Ng PC, Henikoff S. SIFT: predicting amino acid changes that affect protein function. Nucleic Acids Res. 2003;31(13):3812-4.

26. Adzhubei IA, Schmidt S, Peshkin L, Ramensky VE, Gerasimova A, Bork P, et al. A method and server for predicting damaging missense mutations. Nature Methods. 2010;7(4):248-9.

27. Van de Haar J, Canisius S, Yu MK, Voest EE, Wessels LFA, Ideker T. Identifying Epistasis in Cancer Genomes: A Delicate Affair. Cell. 2019;177(6):1375-83.

28. Goldman MJ, Craft B, Hastie M, Repecka K, McDade F, Kamath A, et al. Visualizing and interpreting cancer genomics data via the Xena platform. Nature Biotechnology. 2020;38(6):675-8.

29. Cortes-Ciriano I, Lee S, Park WY, Kim TM, Park PJ. A molecular portrait of microsatellite instability across multiple cancers. Nat Commun. 2017;8:15180.

30. Doll R. The Age Distribution of Cancer: Implications for Models of Carcinogenesis. Journal of the Royal Statistical Society Series A (General). 1971;134(2):133.

31. Ritchie ME, Phipson B, Wu D, Hu Y, Law CW, Shi W, et al. limma powers differential expression analyses for RNA-sequencing and microarray studies. Nucleic Acids Res. 2015;43(7):e47.

32. Zhou X, Edmonson MN, Wilkinson MR, Patel A, Wu G, Liu Y, et al. Exploring genomic alterations in pediatric cancer using ProteinPaint. Cancer Res. 2016;76.

33. Mas-Ponte D, McCullough M, Supek F. Spectrum of DNA mismatch repair failures viewed through the lens of cancer genomics and implications for therapy. Clin Sci (Lond). 2022;136(5):383-404.

34. Akagi K, Oki E, Taniguchi H, Nakatani K, Aoki D, Kuwata T, et al. Real-world data on microsatellite instability status in various unresectable or metastatic solid tumors. Cancer Science. 2021;112(3):1105-13.

35. Kaplan AR, Glazer PM. Impact of hypoxia on DNA repair and genome integrity. Mutagenesis. 2020;35(1):61-7.

36. Mihaylova VT, Bindra RS, Yuan JL, Campisi D, Narayanan L, Jensen R, et al. Decreased expression of the DNA mismatch repair gene Mlh1 under hypoxic stress in mammalian cells. Mol Cell Biol. 2003;23(9):3265-73.

37. Lu Y, Wajapeyee N, Mitchell, Peter. Silencing of the DNA Mismatch Repair Gene MLH1 Induced by Hypoxic Stress in a Pathway Dependent on the Histone Demethylase LSD1. Cell Reports. 2014;8(2):501-13.

38. Chen HB, Yan Y, Davidson TL, Shinkai Y, Costa M. Hypoxic stress induces dimethylated histone H3 lysine 9 through histone methyltransferase G9a in mammalian cells. Cancer Res. 2006;66(18):9009-16.

39. Duan C. Hypoxia-inducible factor 3 biology: complexities and emerging themes. Am J Physiol Cell Physiol. 2016;310(4):C260-9.

40. Yang J, Harris AL, Davidoff AM. Hypoxia and Hormone-Mediated Pathways Converge at the Histone Demethylase KDM4B in Cancer. International Journal of Molecular Sciences. 2018;19(1).

41. Thambirajah AA, Wade MG, Verreault J, Buisine N, Alves VA, Langlois VS, et al. Disruption by stealth-Interference of endocrine disrupting chemicals on hormonal crosstalk with thyroid axis function in humans and other animals. Environ Res. 2022;203.

42. Ogino S, Goel A. Molecular classification and correlates in colorectal cancer. J Mol Diagn. 2008;10(1):13-27.

43. Mal R, Magner A, David J, Datta J, Vallabhaneni M, Kassem M, et al. Estrogen Receptor Beta (ER beta): A Ligand Activated Tumor Suppressor. Front Oncol. 2020;10.

44. Lourbopoulos AI, Mourouzis IS, Trikas AG, Tseti IK, Pantos CI. Effects of Thyroid Hormone on Tissue Hypoxia: Relevance to Sepsis Therapy. J Clin Med. 2021;10(24).

45. Ren B, Zhu Y. A New Perspective on Thyroid Hormones: Crosstalk with Reproductive Hormones in Females. Int J Mol Sci. 2022;23(5).

46. Tsutsumi R, Webster NJG. GnRH Pulsatility, the Pituitary Response and Reproductive Dysfunction. Endocr J. 2009;56(6):729-37.

47. Frederiksen H, Johannsen TH, Andersen SE, Albrethsen J, Landersoe SK, Petersen JH, et al. Sex-specific Estrogen Levels and Reference Intervals from Infancy to Late Adulthood Determined by LC-MS/MS. J Clin Endocrinol Metab. 2020;105(3):754-68.

48. Taylor PN, Albrecht D, Scholz A, Gutierrez-Buey G, Lazarus JH, Dayan CM, et al. Global epidemiology of hyperthyroidism and hypothyroidism. Nat Rev Endocrinol. 2018;14(5):301-16.

49. Krashin E, Piekielko-Witkowska A, Ellis M, Ashur-Fabian O. Thyroid Hormones and Cancer: A Comprehensive Review of Preclinical and Clinical Studies. Front Endocrinol (Lausanne). 2019;10:59.

Table 1. Sex-biased mutated genes.

Gene	Chromosome	Cancer	Female samples +/-	Male samples +/-	Relative risk (f/m)	LRT P value
CASP8	2	HNSC	23/108	19/332	3.24	3.85e-10
RBM10	X	LUAD	9/255	18/205	0.42	3.52e-4
SELP	1	SKCM	13/149	8/249	2.58	7.71e-3
SPAG17	1		17/145	13/244	2.07	7.71e-3
DNAH7	2	STAD	13/131	11/259	2.21	4.70e-2
LARP4B	10		13/131	8/262	3.05	4.27e-2
PGM5	9		13/131	8/262	3.05	4.27e-2
PTEN	10		14/130	12/258	2.19	4.70e-2

"Female samples +/-" and "Male samples +/-" refer to the numbers of samples from women or men that did or did not include a sex-biased gene mutation. "Relative risk (f/m)" represents the female-to-male relative risk of gene mutation frequency. "LRT P value" is the P value obtained from the likelihood ratio test, adjusted using the Benjamini-Hochberg method.

Fig. 1: Cancer incidence curves and prevalence of nonparallel patterns.

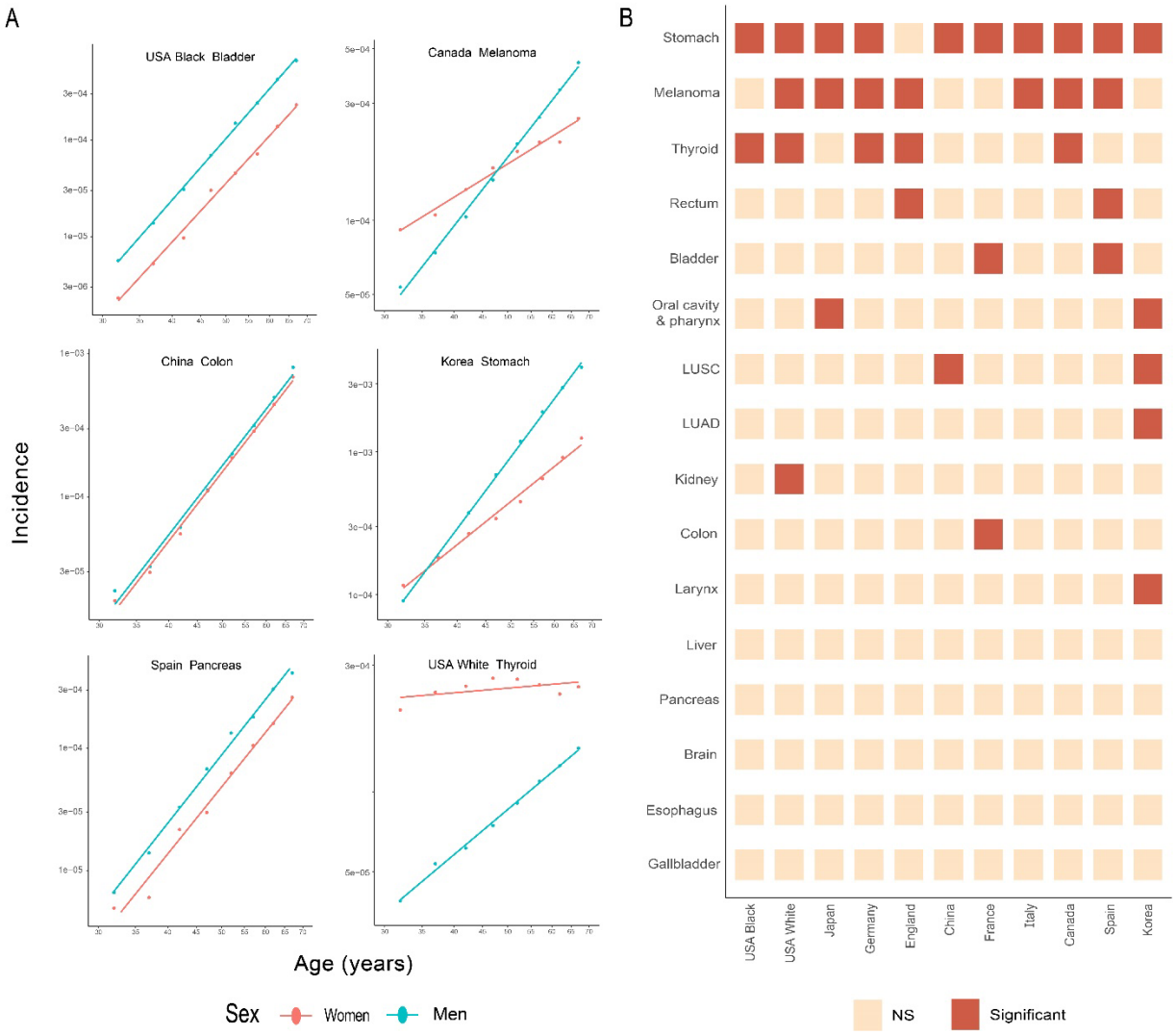

(A) Examples of parallel and nonparallel patterns. Both axes are on a logarithmic scale. Parallel patterns are shown on the left; nonparallel patterns are shown on the right. Incidences and fitted curves for women are shown in red; incidences and fitted curves for men are shown in blue. (B) Prevalence of significant nonparallel patterns in major cancer types according to region or ethnicity. Significant nonparallel patterns are shown in red; non-significant (NS) nonparallel patterns are shown in light yellow.

Fig. 2: Sex bias in tissue environments and nonparallel patterns in adrenal gland cancer.

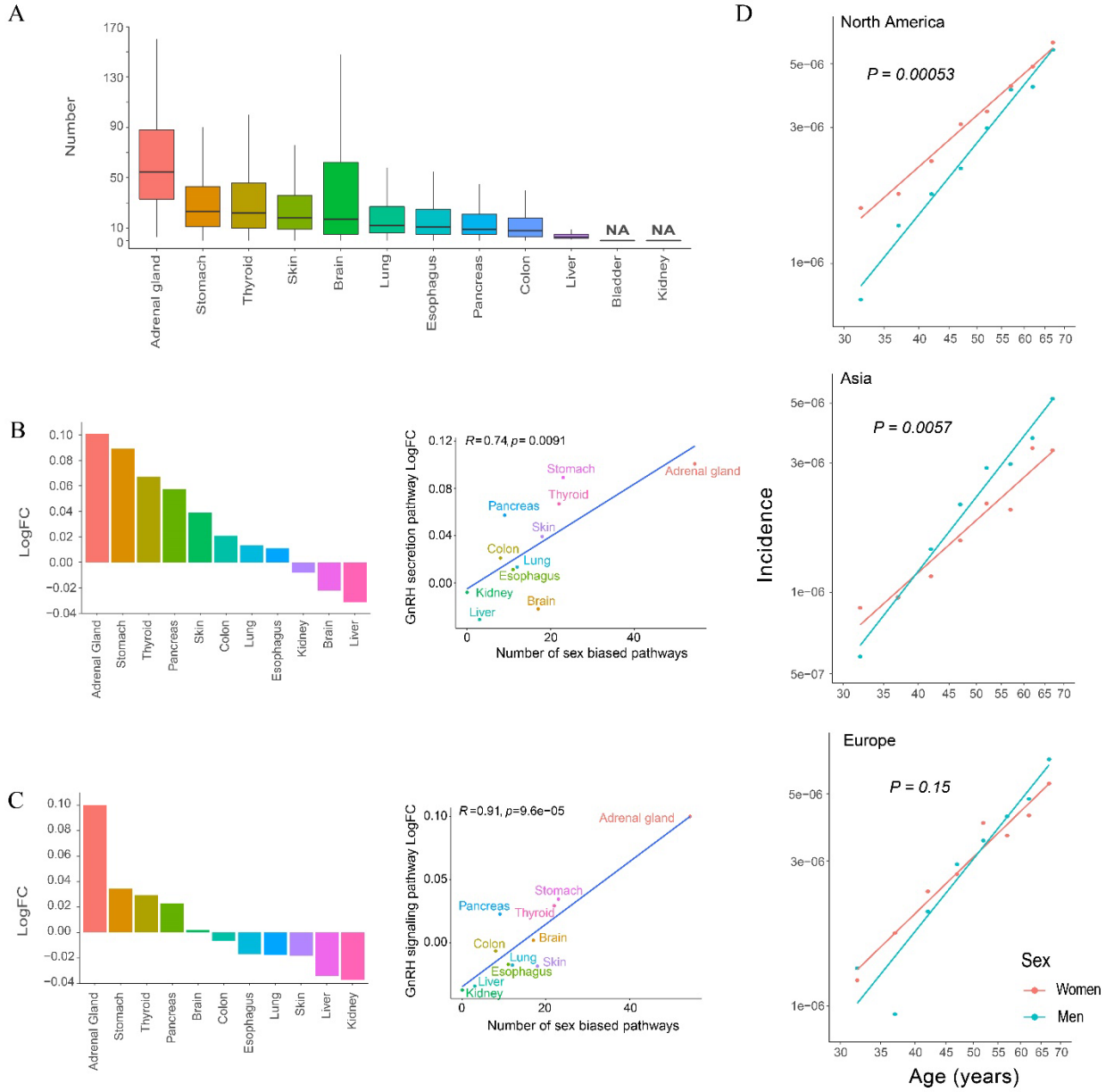

(A) Number of sex-biased pathways expressed in each tissue. The results of bladder and kidney analyses were regarded as not available (NA) because of small sample size. (B and C) Female-to-male log fold changes of GnRH secretion and GnRH signaling pathways among tissues. The results of bladder analyses were excluded because of small sample size. (D) Nonparallel patterns in adrenal gland cancer. Regional cohorts within a single continent were merged to form a continental cohort.

Fig. 3: Mutational spectra of *PTEN*, *PGM5*, and *LARP4B*.

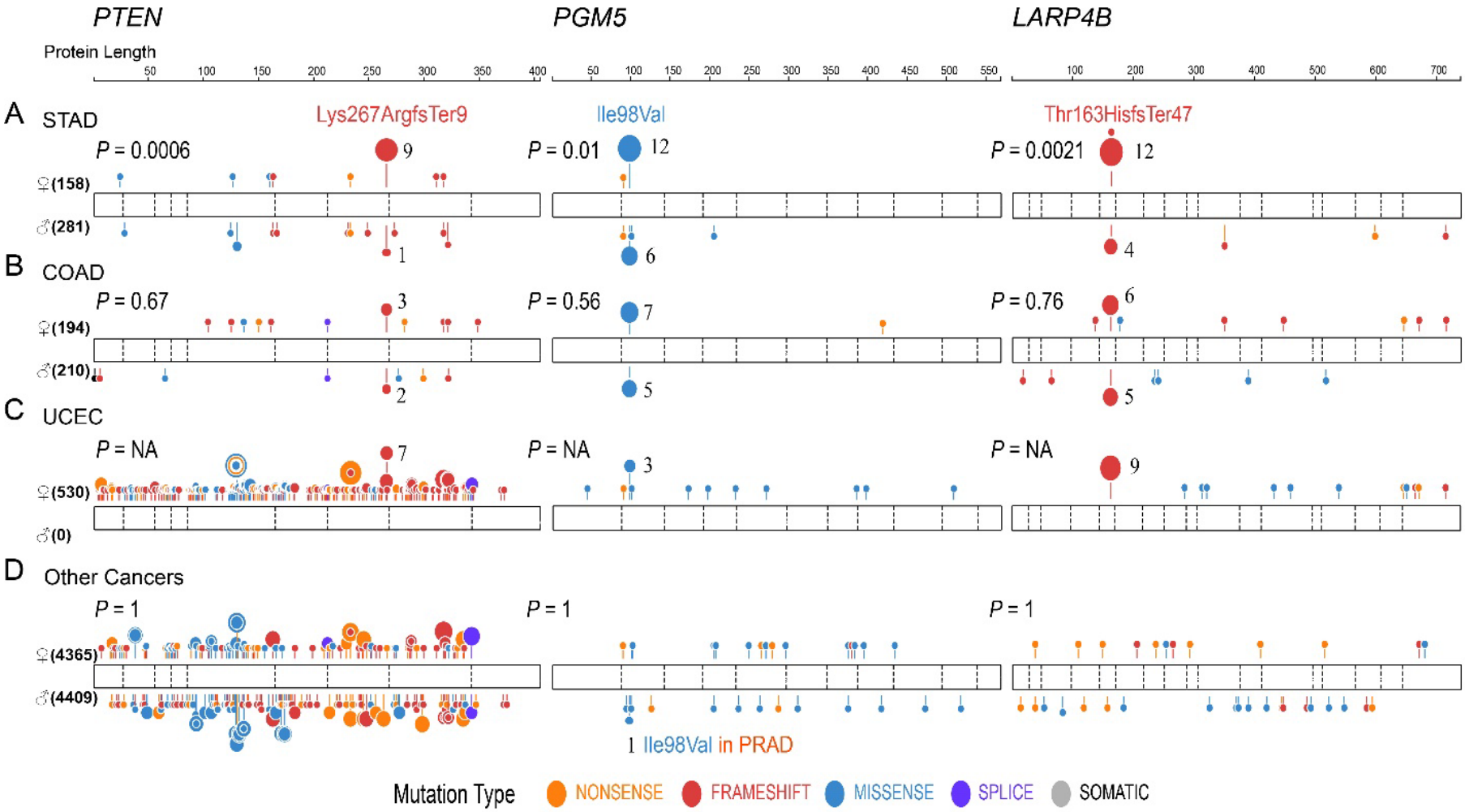

P values above gene body on the left denote statistical significance of hotspot sex bias. Because UCEC is only present in women, the P value is regarded as NA. The numbers of female and male samples for each cancer are indicated on the left in each row. Mutation types are shown in different colors and are annotated at the bottom of the figure.

Fig. 4: Correlations among HIF, *ESR1*, and THR.

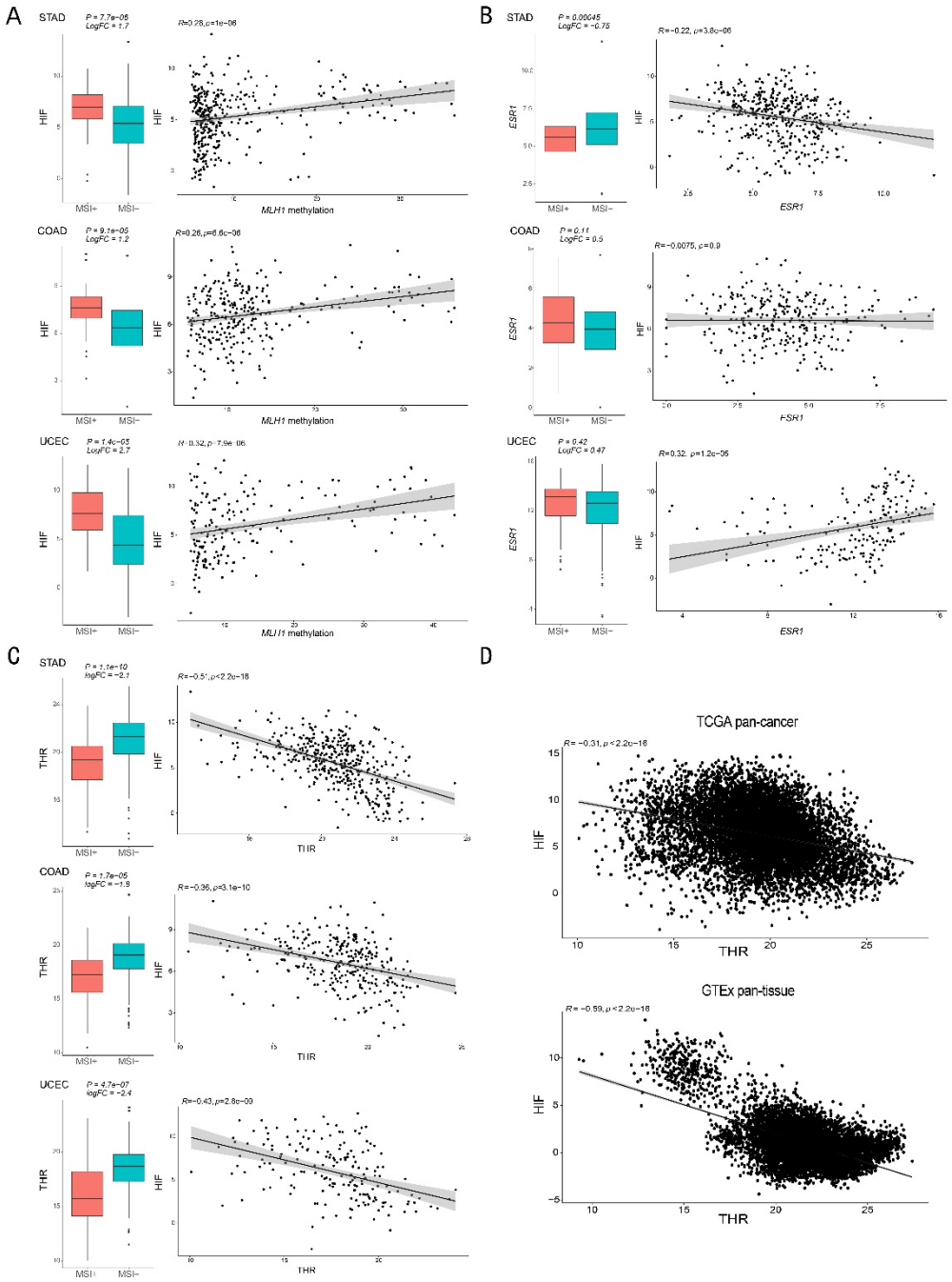

(A) Comparison of HIF levels between MSI+ and MSI- samples, and correlations between HIF level and *MLH1* methylation level across STAD, COAD, and UCEC. (B) Comparison of *ESR1* levels between MSI+ and MSI- samples, and correlations between HIF level and *ESR1* level across STAD, COAD, and UCEC. (C) Comparison of THR levels between MSI+ and MSI- samples, and correlations between HIF level and THR level across STAD, COAD, and UCEC. (D) Correlations between HIF level and THR level in pan-cancer and pan-tissue analyses. In all dot plots, *R* represents the Pearson correlation coefficient; P values were obtained using Student's t-test.

Fig. 5: HIF, *ESR1*, and THR expression signatures in TCGA cancers and the potential contributions of imbalances in estrogen and TH to carcinogenesis.

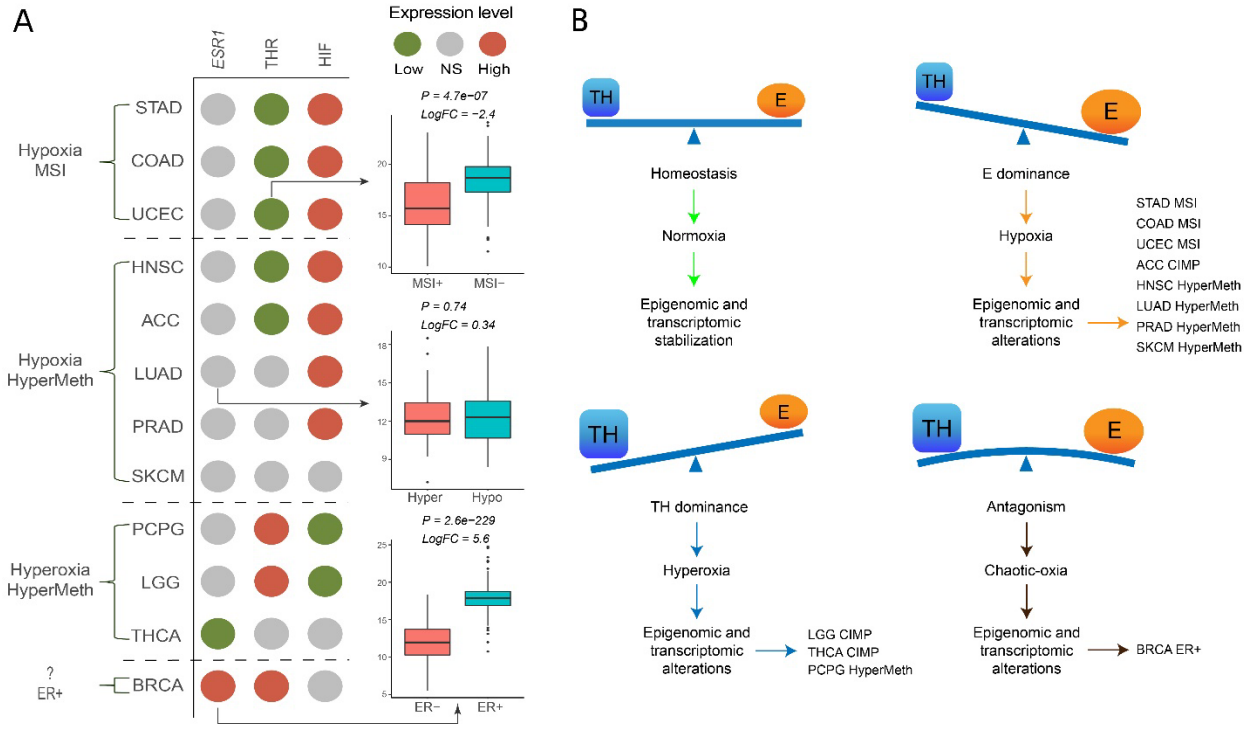

(A) Comparative expression signatures of *ESR1*, THR, and HIF are represented by colored dots. Red dots indicate significantly elevated expression, green dots indicate significantly reduced expression, and gray dots indicate no significant difference in expression when MSI+, HyperMeth, and ER+ cancers are compared with control cancers. Boxplots on the right are representative examples to illustrate the meaning of the dots. LGG: low-grade glioma, THCA: thyroid carcinoma. (B) The relationship between estrogen (E) and TH is illustrated by a seesaw diagram. In a state of homeostasis, the levels of E and TH are in balance. When this balance is disrupted, epigenomic and transcriptomic alterations can occur in affected tissues. These alterations can lead to changes in the tissue environment and function as a selective pressure, thereby inducing specific cancer subtypes.

Supplementary Information

Fig. S1. Mutational spectra of other sex-biased mutated genes in specific cancers.

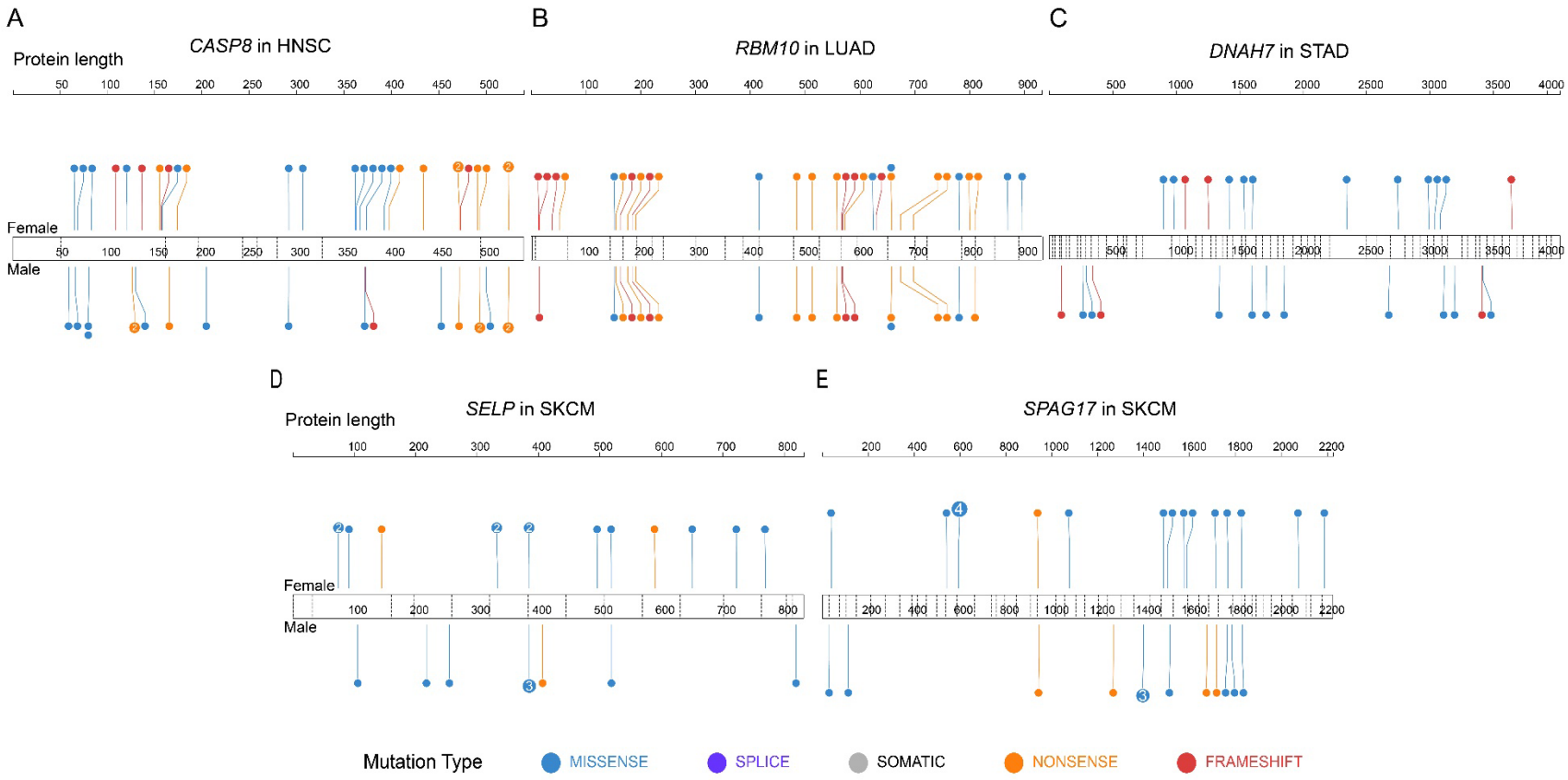

Fig. S2. *MLH1* expression in HOTSPOT+ and HOTSPOT- groups.

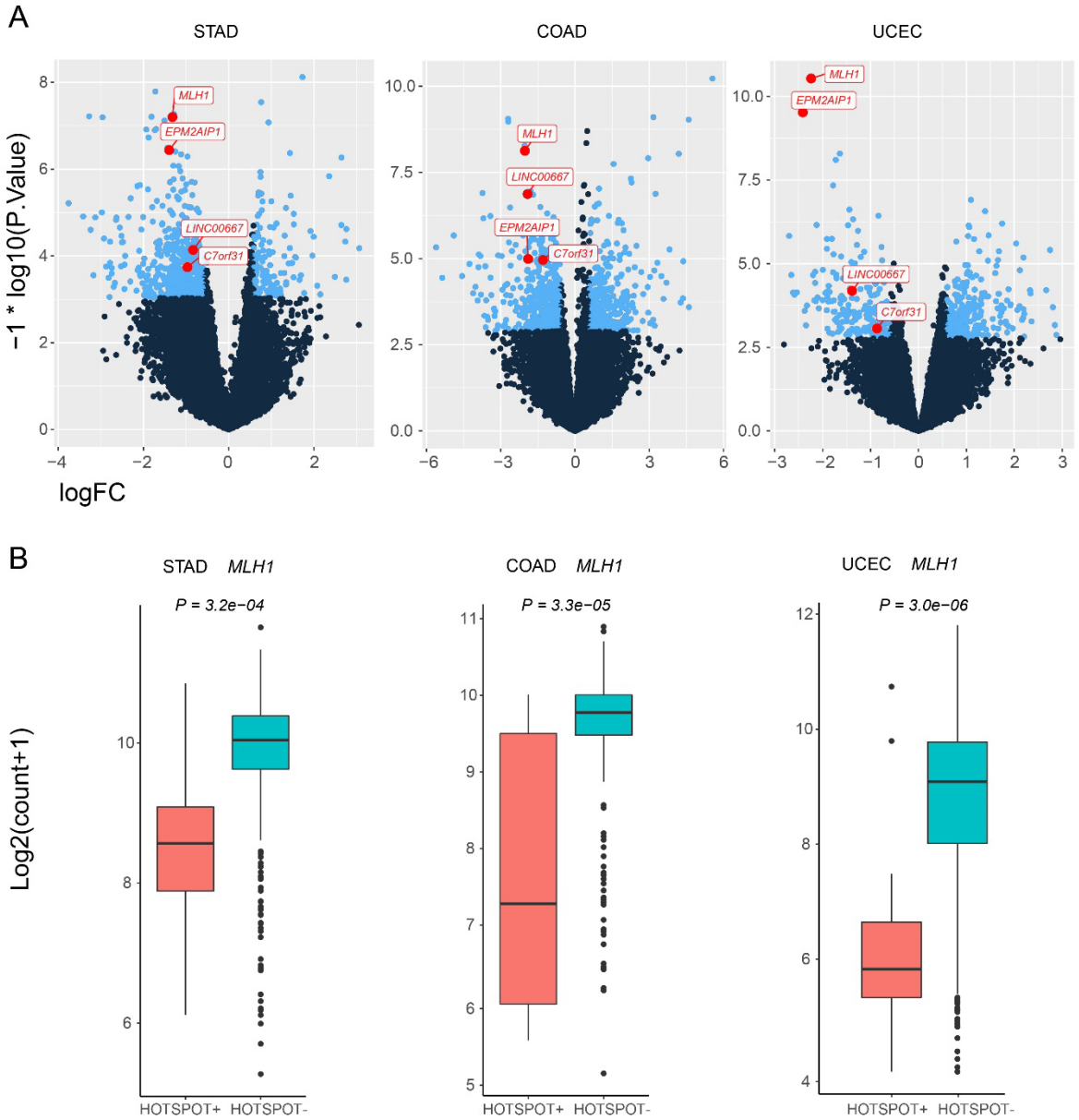

Analyses of DEGs were conducted between HOTSPOT+ and HOTSPOT- groups in STAD, COAD, and UCEC using Limma. The volcano plots are shown in figure A, and four significantly genes are denoted in red. *MLH1* expression is shown in the figure B. P values shown are adjusted P values obtained using Limma.

Fig. S3. Correlations between HIF and *ESR1*.

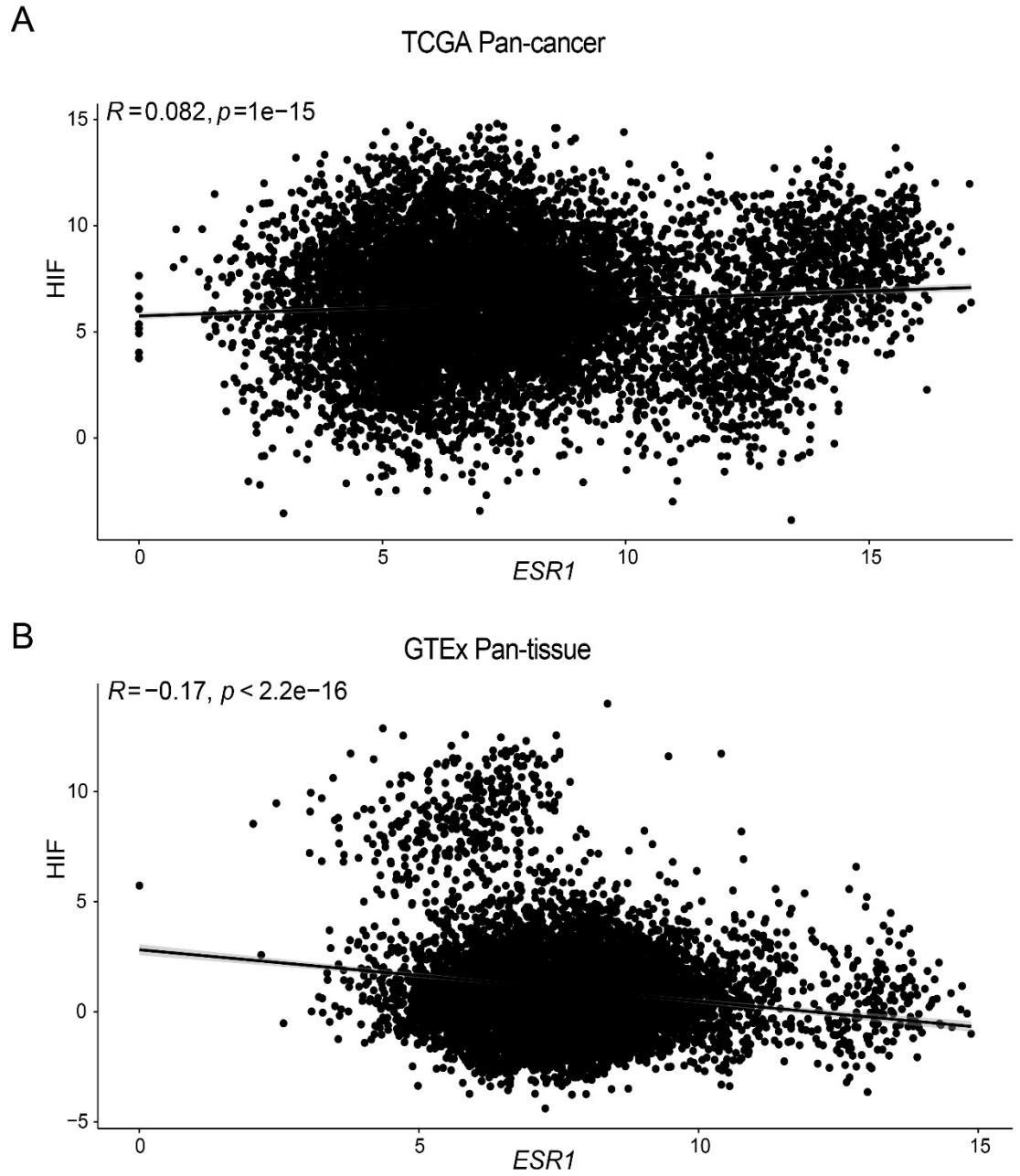

Correlations between HIF level and *ESR1* level in pan-cancer analysis of TCGA data and in pan-tissue analysis of GTEx data. *R* represents the Pearson correlation coefficient; P values were obtained using Student's t-test.

Fig. S4. Boxplot matrix of *ESR1*, *ESR2*, *THRA*, *THRB*, *HIF1A*, and *HIF3A*.

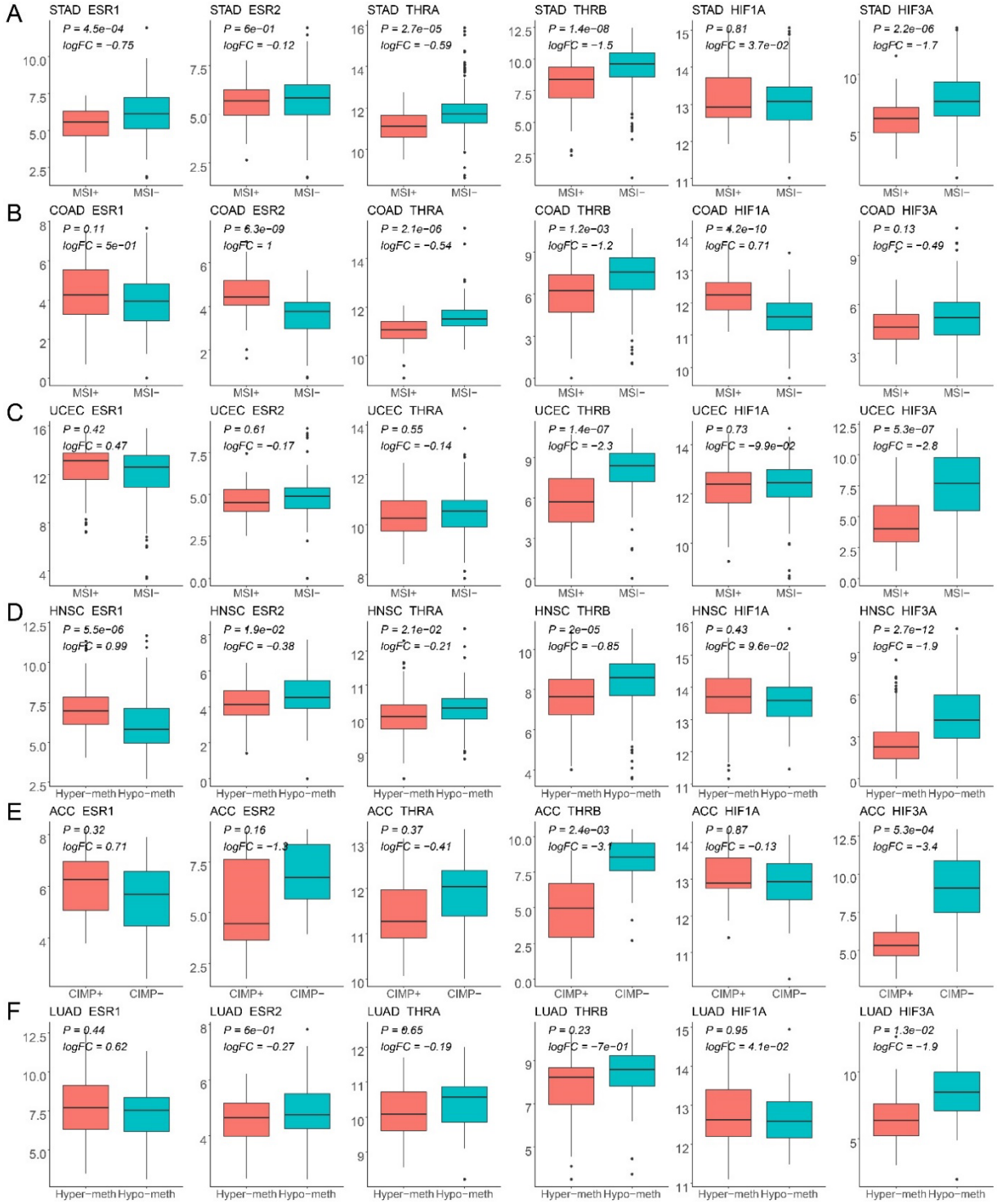

Boxplots of the six genes mentioned in the main text, comparing gene expression between two groups: MSI+ versus MSI-, HyperMeth versus HypoMeth across STAD, COAD, UCEC, HNSC,

ACC and LUAD. The adjusted P value and log fold change shown in the figure were obtained using Limma.

Fig. S5. Boxplot matrix of *ESR1*, *ESR2*, *THRA*, *THRB*, *HIF1A*, and *HIF3A*.

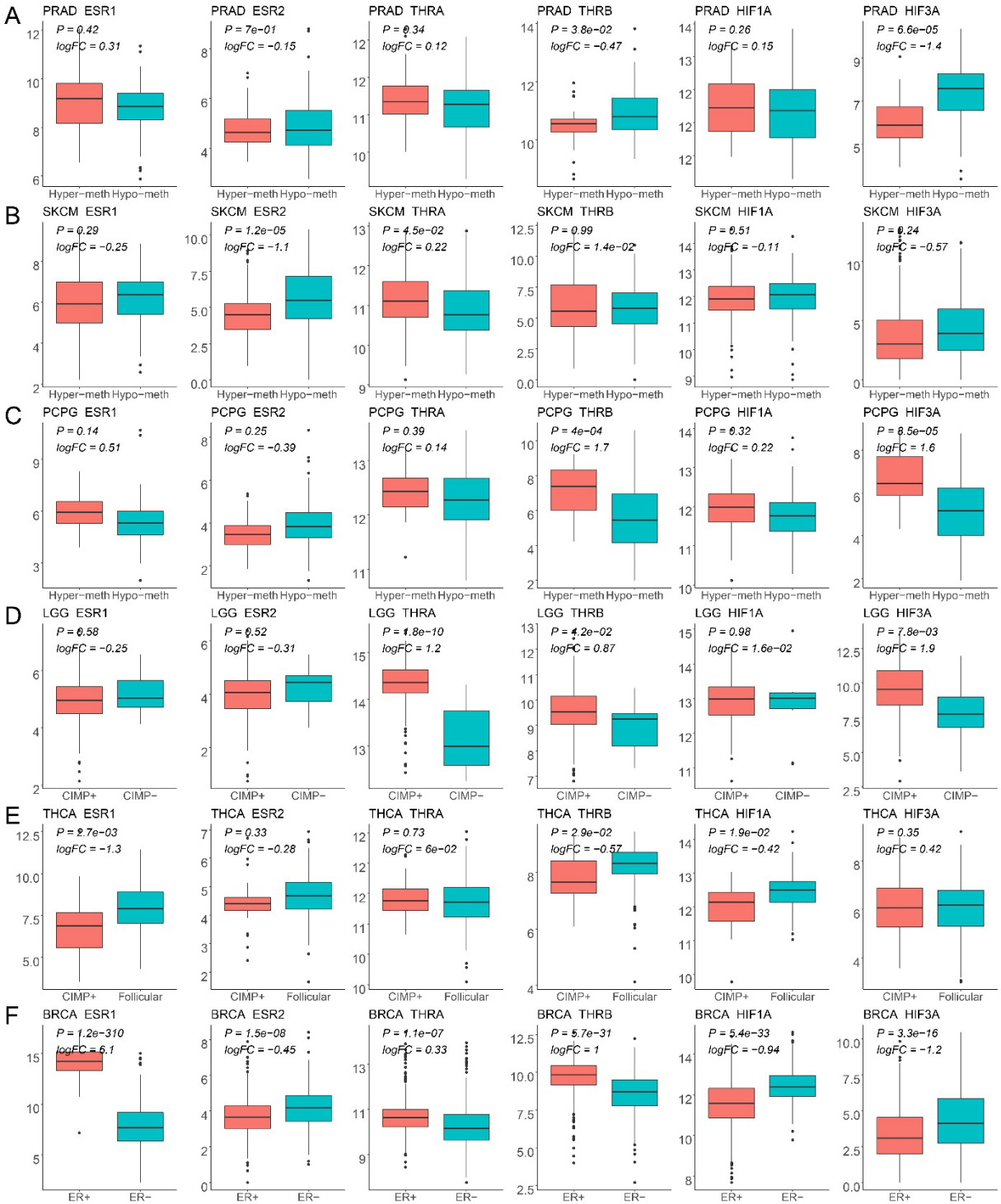

Boxplots of the six genes mentioned in the main text, comparing gene expression between two groups: HyperMeth versus HypoMeth, and ER+ versus ER- across PRAD, SKCM, PCPG, LGG,

THCA and BRCA. The adjusted P value and log fold change shown in the figure were obtained using Limma.

Fig. S6. Boxplot matrix corresponding to Fig. 5A.

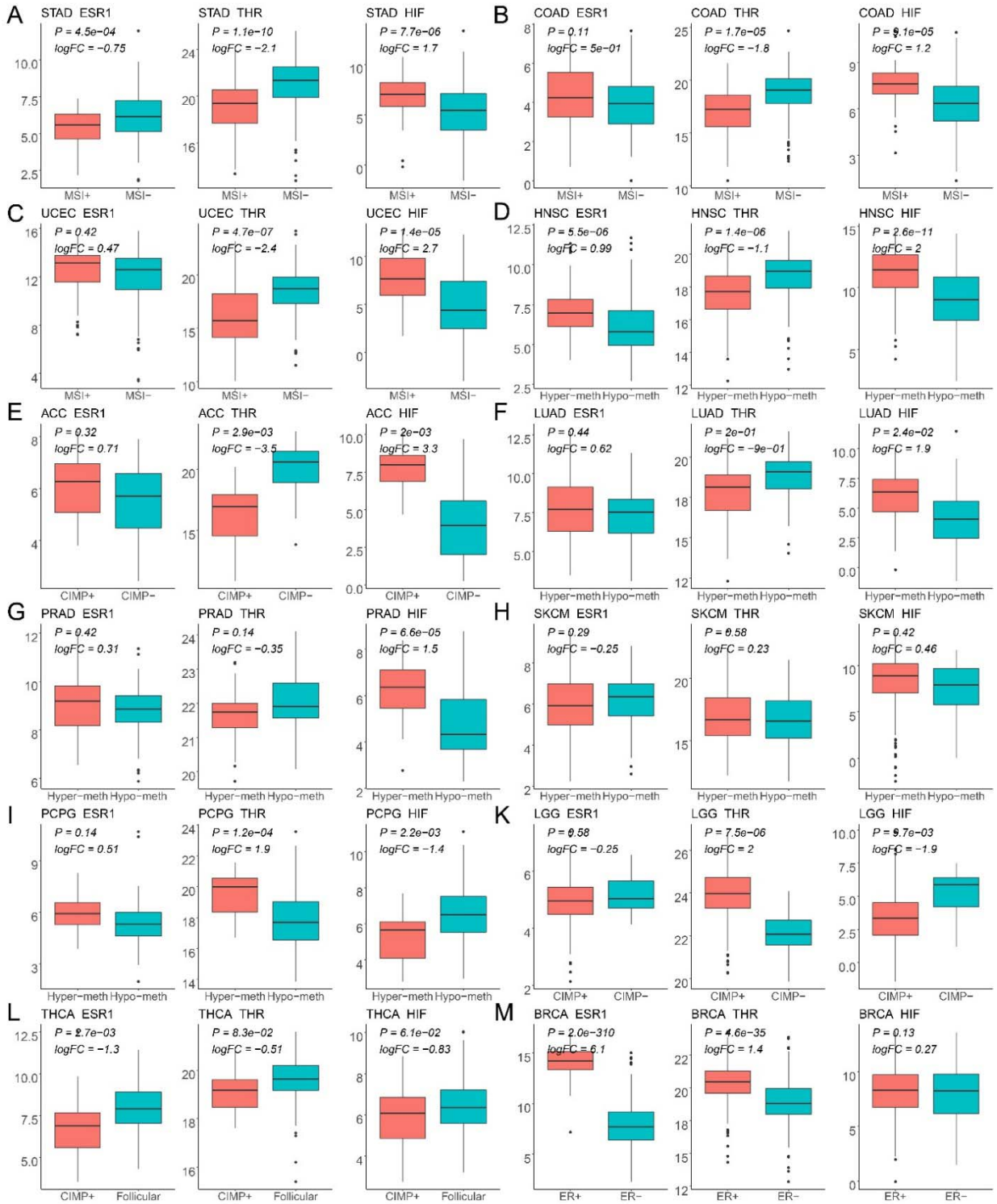

Each boxplot corresponds to each dot in Figure 5A and compares gene expression between two groups: MSI+ versus MSI-, HyperMeth versus HypoMeth, and ER+ versus ER-. The adjusted P value and log fold change shown in the figure were obtained using Limma. (A-M) Dot plots from STAD to BRCA.

Fig. S7. Correlations of THR with *HIF1A* and *HIF3A* in pan-tissue analyses.

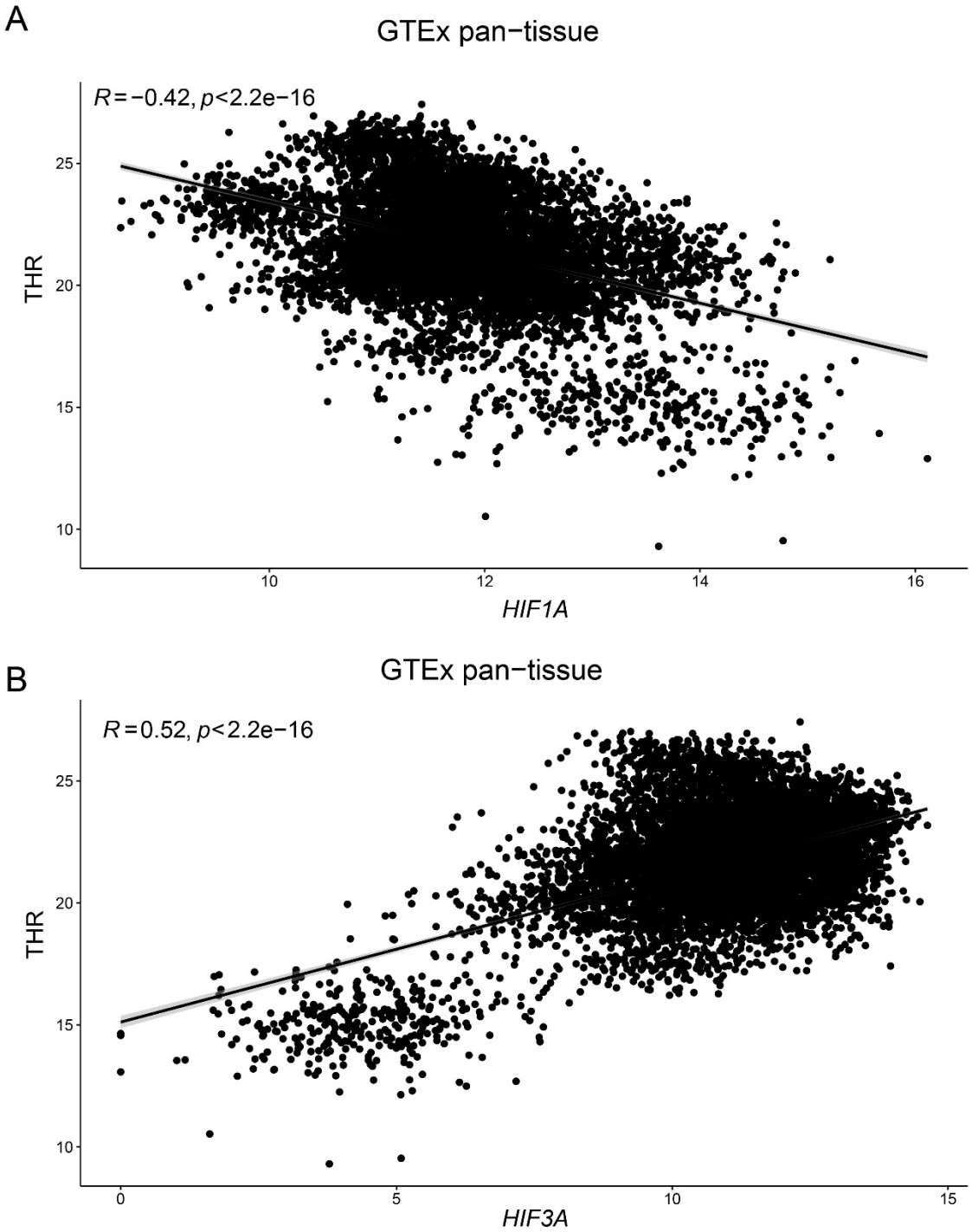

R represents the Pearson correlation coefficient; P values were obtained using Student's t-test.

Fig. S8. Correlations of THR with *HIF1A* and *HIF3A* in pan-cancer analyses.

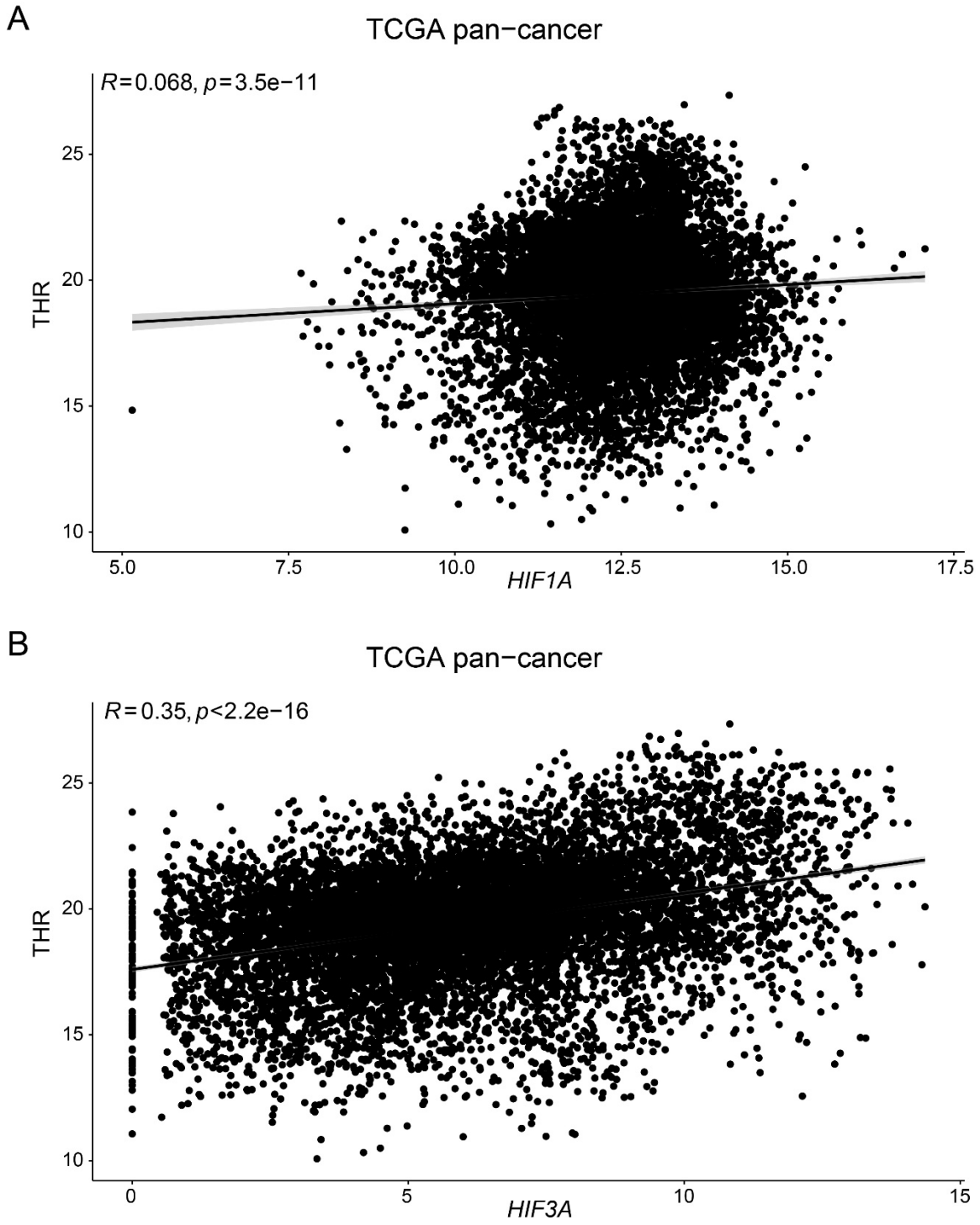

R represents the Pearson correlation coefficient; P values were obtained using Student's t-test.

Table S1. Sample sizes for each tissue in GTEx data

Tissue	Female	Male	Total
Bladder	3	6	9
Kidney	5	22	27
Liver	33	77	110
Skin	190	366	556
Colon	124	180	304
Stomach	73	99	172
Pancreas	72	93	165
Lung	100	187	287
Thyroid	105	173	278
Brain	353	783	1136
Esophagus	234	415	649
Adrenal gland	57	70	127

Table S2. Tissue-specific sex-biased expression of the GnRH secretion pathway based on GTEx data

Tissue	P value	LogFC
Adrenal gland	0.030899	0.100831
Stomach	0.012977	0.08919
Thyroid	0.009457	0.066973
Pancreas	0.112046	0.057273
Skin	0.068307	0.039208
Colon	0.414889	0.020896
Lung	0.565389	0.013314
Esophagus	0.533371	0.011119
Kidney	0.955948	-0.00815
Brain	0.269388	-0.02215
Liver	0.579539	-0.03118

P values shown are adjusted P values obtained using Limma.

Table S3. Tissue-specific sex-biased expression of the GnRH signaling pathway based on GTEx data

Tissue	P value	LogFC
Adrenal gland	0.002109	0.100018
Stomach	0.221583	0.034591
Thyroid	0.167189	0.029276
Pancreas	0.409804	0.022836
Brain	0.885571	0.002091
Colon	0.683874	-0.00639
Esophagus	0.196701	-0.01705
Lung	0.402423	-0.0175
Skin	0.217595	-0.01834
Liver	0.482774	-0.03411
Kidney	0.702808	-0.03714

P values shown are adjusted P values obtained using Limma.

Table S4. Co-occurrence and mutual exclusivity analysis of the three hotspots

Hotspot1	Hotspot2	Co-occurring samples	Hotspot1-only samples	Hotspot2-only samples	No hotspot samples	P value	Direction
*PTEN*_267	*PGM5*_98	5	22	22	1162	2.2e-4	Co-occur
*PTEN*_267	*LARP4B*_163	5	22	20	1164	1.5e-4	Co-occur
*PGM5*_98	*LARP4B*_163	5	22	20	1164	1.5e-4	Co-occur

Fisher's exact test was performed on three pairs of the three hotspot mutations. All pairs tended to co-occur as indicated in the "Direction" column.

Table S5. Proportions of subtypes in TCGA data.

Cancer	Sex	MSI+/ HyperMeth/ ER+ samples	Total samples	Ratio	Relative risk (f/m)	P value
STAD	Male	40	252	0.15873	1.923664	0.0013
	Female	40	131	0.305344		
COAD	Male	30	172	0.174419	1.235928	0.412533
	Female	36	167	0.215569		
UCEC	Female	124	507	0.244576	NA	NA
LGG	Male	132	135	0.977778	0.93905	0.063995
	Female	101	110	0.918182		
GBM	Male	10	17	0.588235	0.772727	0.760509
	Female	5	11	0.454545		
ACC	Male	7	16	0.4375	0.825397	0.830716
	Female	13	36	0.361111		
THCA	Male	13	42	0.309524	0.590237	0.145401
	Female	19	104	0.182692		
SKCM	Male	96	204	0.470588	0.962891	0.843433
	Female	58	128	0.453125		
PCPG	Male	46	60	0.766667	1.032609	0.893141
	Female	57	72	0.791667		
HNSC	Male	95	203	0.46798	0.702909	0.050884
	Female	25	76	0.328947		
LUAD	Male	35	56	0.625	1.134545	0.460331
	Female	39	55	0.709091		
PRAD	Male	182	333	0.546547	NA	NA
BRCA	Female	770	1043	0.738255	NA	NA

P values were obtained using z-test for proportions.

Table S6. Proportions of MSI subtypes in the work by Akagi et al *(24)*.

Cancer	Sex	MSI+ samples	Total samples	Ratio	Relative risk (f/m)	P value
Gastric	Male	60	1250	4.8%	1.63	0.013
	Female	45	574	7.8%		
Colorectal	Male	186	5676	3.3%	1.37	0.0026
	Female	185	4138	4.5%		
Endometrial	Female	234	1389	16.8%	NA	NA

For gastric and colorectal cancers, the proportions of MSI subtypes were significantly higher in women than in men. P values were obtained using z-test for proportions.

Table S7 Mutation distributions of sex-biased mutated genes

Gene	Cancer	Group	Samples with mutation	Wild-type samples	P value
CASP8	HNSC	HyperMeth	17	142	7.97e-4
		HypoMeth	1	119	
RBM10	LUAD	HyperMeth	3	34	0.398
		HypoMeth	3	71	
SELP	SKCM	HyperMeth	17	161	0.0117
		HypoMeth	4	150	
SPAG17	SKCM	HyperMeth	10	168	0.387
		HypoMeth	13	141	
DNAH7	STAD	MSI+	12	68	3.45e-4
		MSI-	10	293	
PGM5	STAD	MSI+	18	62	1.73e-12
		MSI-	1	302	
LARP4B	STAD	MSI+	17	63	7.56e-11
		MSI-	2	301	
PTEN	STAD	MSI+	12	68	9.79e-05
		MSI-	8	295	

Mutation distributions of sex-biased mutated genes were compared between groups as shown in table. P values were obtained using Fisher's exact test. Hotspot mutations of *PGM5*, *LARP4B*, and *PTEN* exclusively occurred in MSI+ cancers, as discussed in main text.

Data S1. Results of nonparallel pattern tests

Data S2. Results of sex-biased expressed pathway analysis in GTEx data

Data S3. Results of sex-biased mutated gene analysis in TCGA data

Data S4. Results of hotspot-grouped DEG analysis in STAD, COAD, and UCEC

Data S5. Results of subtype-grouped DEG analysis in TCGA data